Deep-Sea Research I 56 (2009) 471–494

Contents lists available at ScienceDirect

Deep-Sea Research I

journal homepage: www.elsevier.com/locate/dsri

The influence of bottom topography on the decay of modeled Agulhas rings

L. de Steur [a,*], P.J. van Leeuwen [b]

[a] Norwegian Polar Institute, Hjalmar Johansensgate 14, 9296 Tromsø, Norway
[b] Institute for Marine and Atmospheric research Utrecht (IMAU), Princetonplein 5, 3584 CC Utrecht, The Netherlands

ARTICLE INFO

Article history:
Received 14 November 2007
Received in revised form
22 November 2008
Accepted 24 November 2008
Available online 6 December 2008

Keywords:
Agulhas rings
Topographic ridge
Numerical modeling
Energy conversion
Passive tracer

ABSTRACT

The influence of a large meridional submarine ridge on the decay of Agulhas rings is investigated with a 1 and 2-layer setup of the isopycnic primitive-equation ocean model MICOM.

In the single-layer case we show that the SSH decay of the ring is primarily governed by bottom friction and secondly by the radiation of Rossby waves. When a topographic ridge is present, the effect of the ridge on SSH decay and loss of tracer from the ring is negligible. However, the barotropic ring cannot pass the ridge due to energy and vorticity constraints.

In the case of two-layer ring the initial SSH decay is governed by a mixed barotropic–baroclinic instability of the ring. Again, radiation of barotropic Rossby waves is present. When the ring passes the topographic ridge, it shows a small but significant stagnation of SSH decay, agreeing with satellite altimetry observations. This is found to be due to a reduction of the growth rate of the $m = 2$ instability, to conversions of kinetic energy to the upper layer, and to a decrease in Rossby-wave radiation. The energy transfer is related to the fact that coherent structures in the lower layer cannot pass the steep ridge due to energy constraints. Furthermore, the loss of tracer from the ring through filamentation is less than for a ring moving over a flat bottom, related to a decrease in propagation speed of the ring. We conclude that ridges like the Walvis Ridge tend to stabilize a multi-layer ring and reduce its decay.

1. Introduction

After being spawned from the Agulhas Current, large anticyclonic Agulhas rings move into the southeastern Atlantic Ocean where they lose energy and exchange heat and salt with their surroundings (Van Ballegooyen et al., 1994; Duncombe Rae et al., 1996). The Agulhas rings are an important factor in the interocean exchange in the Agulhas region and are shown to contribute to the global thermohaline circulation (Gordon, 1986; De Ruijter et al., 1999; Weijer et al., 2002). The observed decay in sea-surface height (SSH) of Agulhas rings by Schouten et al. (2000) corresponds with the loss of Agulhas ring water which occurs mainly through shedding large filaments of Agulhas ring water as shown in a numerical study by De Steur et al. (2004). The decay of oceanic rings in general is related to a mixed baroclinic/barotropic instability of the rings which has been investigated for a whole set of ring parameters by Drijfhout et al. (2003).

On their way to the Cape Basin into the Atlantic Ocean, Agulhas rings encounter different topographic features such as seamounts, the continental shelf and submarine ridges. The Walvis Ridge, extending from 20°S, 10°E to as far as 34°S, 15°W and having a height up to 2400 m, is the largest of these features. Byrne et al. (1995) and Van Ballegooyen et al. (1994) have shown that the Walvis Ridge has a considerable impact on the evolution of Agulhas rings, such as decreasing their propagation

* Corresponding author. Tel.: +47 77750547.
E-mail address: desteur@npolar.no (L. de Steur).

0967-0637/$ - see front matter © 2008 Elsevier Ltd. All rights reserved.
doi:10.1016/j.dsr.2008.11.009

velocity, altering their general west-northwest course and steering the rings through the deepest parts of the ridge. In addition to these findings, Schouten et al. (2000) observed that the decay rate of the SSH of the rings decreases after crossing the Walvis Ridge. Both Byrne et al. (1995) and Schouten et al. (2000) have suggested that topographic features like the Walvis Ridge or seamounts may have a strong influence on mixing and dissipation of rings.

Many numerical studies have been performed to investigate the behavior of rings in the presence of sloping bottom topography, mainly focusing on the changes in propagation of eddies (Thierry and Morel, 1999; Jacob et al., 2002) or differences between anticyclonic and cyclonic eddies with respect to topography (Smith and O'Brian, 1983). Kamenkovich et al. (1996) varied the vertical structure of eddies in a 2-layer primitive-equation model and showed that baroclinic eddies can cross a shallow modeled ridge, whereas barotropic ones cannot. They also show that in presence of a ridge the amount of transported tracer with an eddy is larger than in the case of a flat bottom, but there is no physical explanation given for this result. Beismann et al. (1999) investigated the migration of rings for a ridge with varying height using a 2-layer quasi-geostrophic model. They found that the lower layer becomes decoupled from the upper layer and only when the rings obtain a state of deep compensation can they cross the topographic obstacle.

The result of Kamenkovich et al. (1996) that the amount of tracer transported by rings moving over a ridge is larger than for rings moving over a flat bottom is in contradiction with suggestions that topography may enhance mixing of thermohaline properties of rings. Here, we investigate the effect of a topographic ridge on the decay of SSH and tracer loss from Agulhas rings more thoroughly, using a primitive-equation isopycnic model and a topographic ridge of realistic dimensions. The main research question dealt with in this paper is which processes are responsible for the mixing of ring water with the environment and the decay of the ring when a topographic ridge is present. This is a natural follow-up of De Steur et al. (2004) in which the decay of a multi-layer ring over a flat bottom case is investigated.

To this end we start with a ring in a barotropic ocean in Section 3, of which the results are compared to those from a 2-layer ring with a significant barotropic component in Section 4. The changes in SSH decay and tracer content are determined for a flat bottom and in presence of a ridge. In Section 2 the numerical model that is used for the experiments as well as the initial conditions are described. The conclusions are summarized and discussed in Section 5.

2. Model setup

The model we use for the experiments is MICOM (Miami Isopycnic Coordinate Ocean Model) version 2.7, as described by Bleck and Smith (1990). We use a 1200×1200 km domain with a horizontal resolution of 5 km. In the 1-layer case we use sponge layers of 50 km (or 10 gridpoints) on all lateral boundaries where the barotropic fields are linearly relaxed towards the initial values. In the 2-layer case we apply doubly periodic boundary conditions on all lateral boundaries. In the 1-layer case there is one layer of 4000 m thickness and in the 2-layer case there are two isopycnal layers of 400 and 3600 mm, respectively, which have potential density anomalies of 26.37 and 27.68 $\mathrm{kg\,m^{-3}}$. The diffusion velocities for momentum dissipation and for mixing of temperature and salinity are 0.5 $\mathrm{cm\,s^{-1}}$ (which are multiplied by the grid distance to obtain the actual coefficients). The coefficient used in deformation-dependent viscosity is 0.5. Diapycnal diffusion is set to zero. Bottom stress is parameterized by a quadratic drag relation with a drag coefficient C_D of 0.0013. All the model runs are performed on the beta-plane. In the 1-layer case two additional experiments are performed to investigate the effect of bottom drag. A passive tracer is initialized within the ring in order to quantify the amount of stirring of ring water from the ring, identical to the method described by De Steur et al. (2004). The topographic ridge is modeled as an idealized, meridional ridge with a zonal Gaussian profile which has a maximum height of 2400 m and an e-folding width of 60 km. The vortex is initialized as an inverted potential vorticity anomaly (PVA) in order to avoid rapid growth of instabilities in the ring (Carton and McWilliams, 1989; Herbette et al., 2003). The only difference is that we neglect the relative vorticity term in the PVA and approximate the layer thickness as

$$h_1(r) = H + H\frac{\Delta Q_0\left(1-\frac{r^2}{R^2}\right)\exp\left(-\frac{r^2}{R^2}\right)}{-f_0+\Delta Q_0\left(1-\frac{r^2}{R^2}\right)\exp\left(-\frac{r^2}{R^2}\right)} \tag{1}$$

where $\Delta Q_0 = -f_0(\Delta h/(\Delta h + H))$. We choose the value of the Coriolis parameter f_0 at the center of the ring to obtain a circular symmetric profile. The total velocities are initialized in cyclogeostrophic balance. For the 1-layer ring, H is the undisturbed layer thickness of 4000 m and Δh is the initial SSH anomaly of 70 cm, giving maximum azimuthal velocities of about 70 cm/s. For the 2-layer ring H is the undisturbed upper layer thickness of 400 m and Δh the maximum interface anomaly of 390 m. The rings have an initial radius R of 100 km. The 2-layer ring has maximum baroclinic velocities of 50 cm/s in the upper layer and 10 cm/s in the lower layer. An additional barotropic component with the same shape as Eq. (1) and equivalent to a barotropic velocity of 15 cm/s is added such that the ring is co-rotating. The initial maximum SSH anomaly of the 2-layer ring is 60 cm. The ring parameters are realistic in that sense that they are simplified for these single and 2-layer cases relative to previous multi-layer modeling studies of Agulhas rings (Drijfhout et al., 2003; De Steur et al., 2004).

3. The 1-layer ring

3.1. *Ring evolution—flat bottom*

We start by describing the evolution for a 1-layer ring and a flat bottom in order to determine the effect of bottom friction. The ring is initialized at 6.5°E, 30.5°S. On average the translation speed of the ring is 5.5 km/day. The evolution of the sea-surface elevation with bottom drag turned in Fig. 1(a) shows that the ring radiates a barotropic Rossby wave at day 30. Both the ring and wave are almost completely dissipated at day 80. When bottom friction is turned off (Fig. 1(b)) the ring dissipates less fast than in the case with bottom drag. At day 80 the ring is still visible in the SSH field and shows two cores. Additional cyclonic and anticyclonic structures have appeared in the domain due to interaction of the Rossby wave with the ring and the boundary.

The passive tracer in the 1-layer case is initialized having a value 1 inside a boundary B defined by the barotropic pressure P_b as $B = P_b^0 + 5\% P_b^{max}$. Outside this boundary the tracer is 0. With bottom friction the evolution of tracer concentration at days 30 and 80 (Fig. 2(a)) shows that tracer is removed from the ring through the development and shedding of large filaments as described in De Steur et al. (2004). With bottom friction turned off, initial filamentation of tracer is identical but at day 80 the tracer filament is much smaller (Fig. 2(b)).

The initial fast decay of the maximum SSH (which corresponds with the center of the ring) as a function of time takes place during the first 30 days (Fig. 3(a)). Hereafter the SSH signal increases slightly again until days 50–60, after which it rapidly decreases. The integrated tracer content of the ring as a function of time shows the same trend (Fig. 3(b)) since the boundary of the ring is determined by SSH. After 85 days the tracer content in the

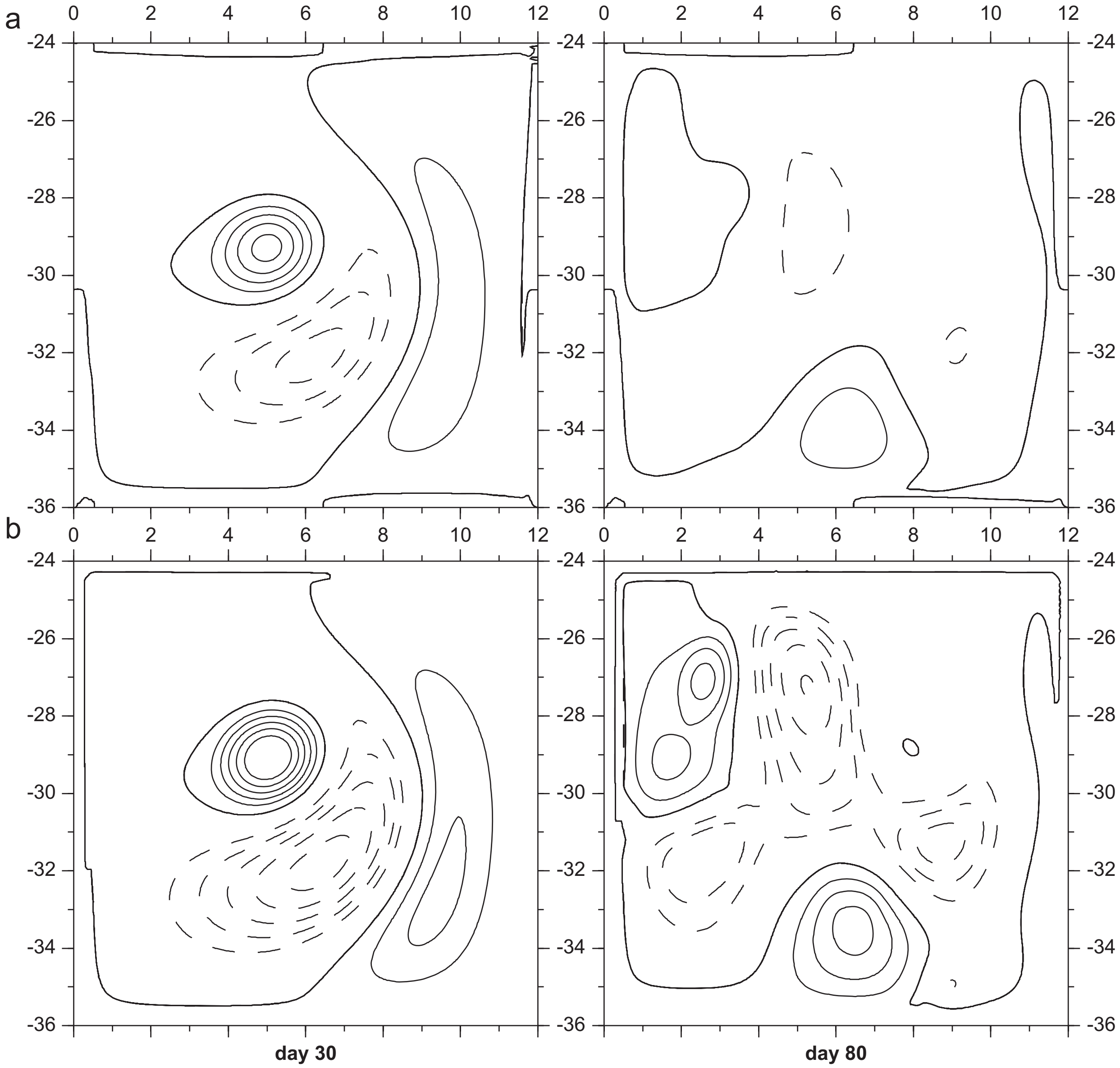

Fig. 1. Sea-surface elevation at days 30 and 80 (contours; interval = 6 cm) for the barotropic ring: (a) flat bottom with bottom drag and (b) flat bottom without bottom drag.

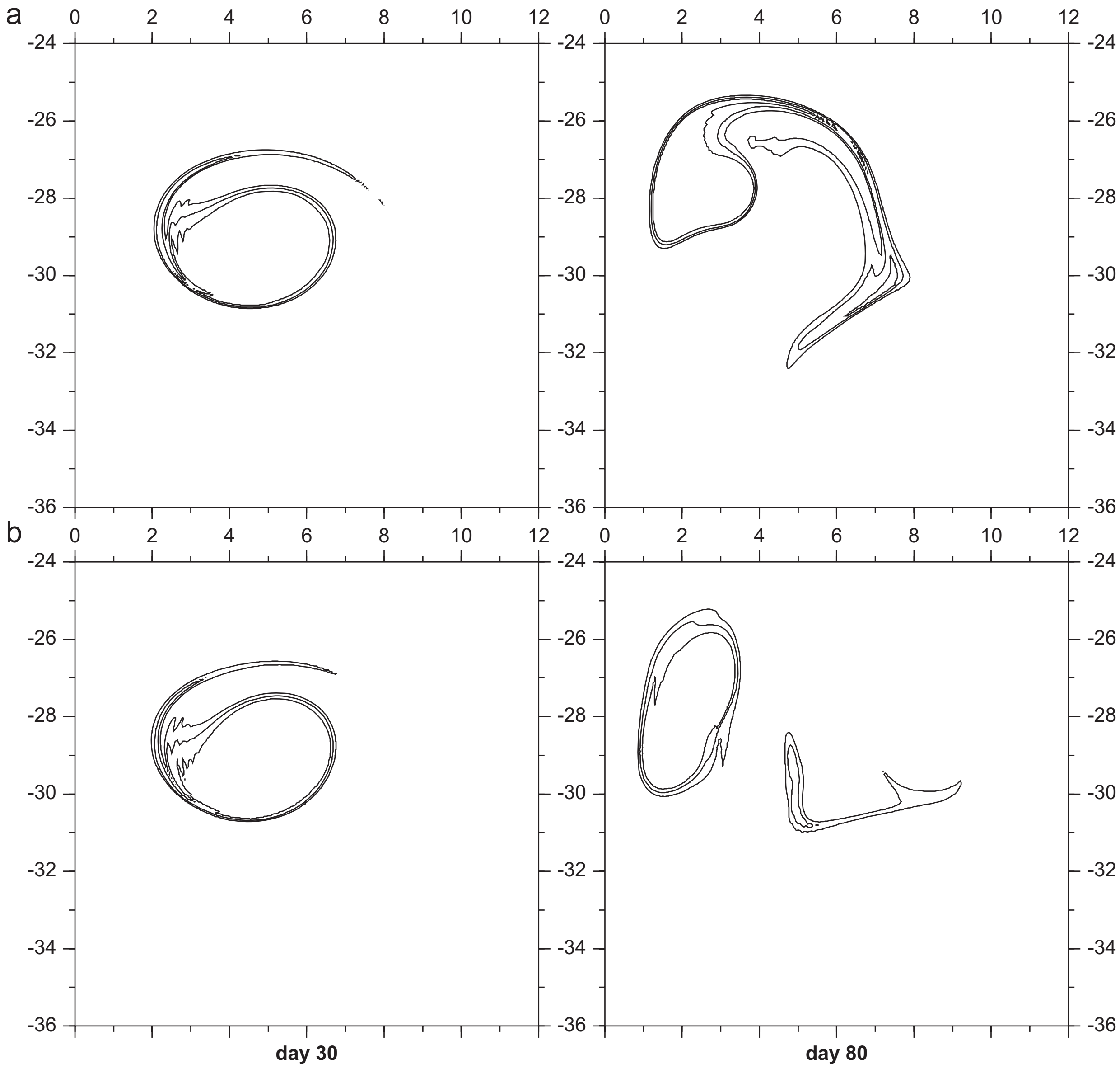

Fig. 2. Tracer concentration at days 30 and 80 (contours; interval = 0.3) for the barotropic ring: (a) flat bottom with bottom drag and (b) flat bottom without bottom drag.

ring is 50% and the ring has reached the sponge layer at the boundary of the domain. Hereafter, as the ring dissipates at the boundary of the domain, the ring boundary and thus tracer content, can no longer be determined. Without bottom friction, the SSH decreases as a function of time is much smaller (Fig. 3(a)) and it shows a large increase of SSH around day 50. Thereafter, SSH decays at the same rate as in the case with bottom drag. The total tracer content of the ring as a function of time shows that there is less tracer leakage from day 60 onwards (Fig. 3(b)), consistent with the fact that a smaller filament is shed from the ring in this case. After 85 days the tracer content of the ring without bottom drag is still 80%.

3.2. *Ring evolution—ridge*

In the presence of a meridional topographic ridge and with bottom friction on, the ring moves slower than in the case of a flat bottom with an average speed of 3.8 km/day. The initial evolution of the ring is similar to that in the flat bottom case, however, after 80 days the ring is blocked by the ridge and it is still clearly visible in SSH (Fig. 4(a)). When bottom drag is turned off, the ring dissipates less fast (Fig. 4(b)). As the ring meets the ridge it develops towards a weak dipolar structure, with the cyclonic part at 4°E, 32°S, which will be discussed in more detail in Section 3.3.2.

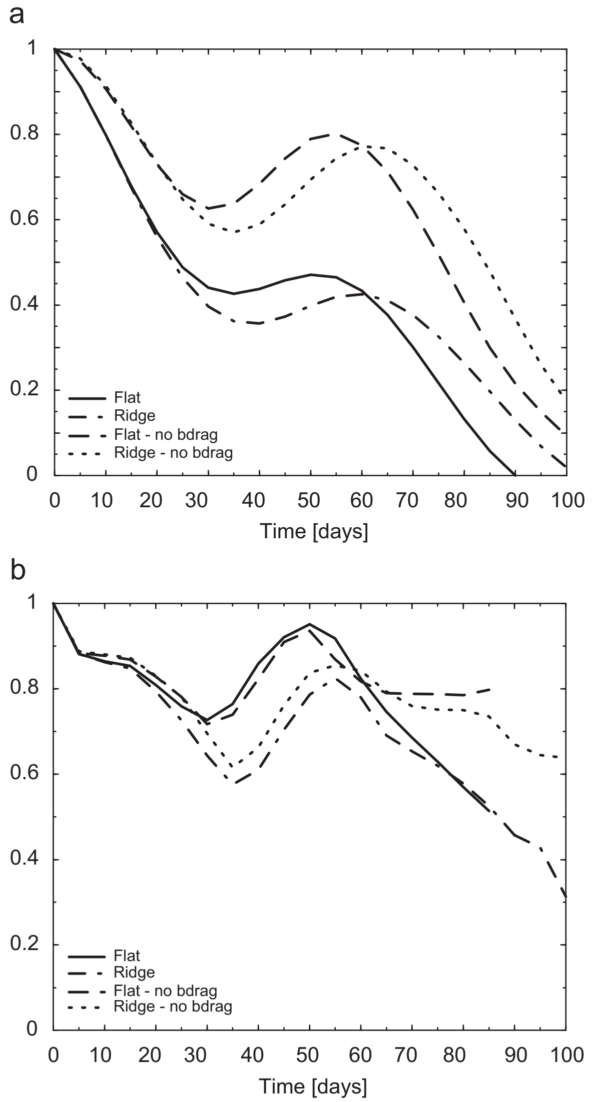

Fig. 3. Decay of the barotropic ring as a function of time: (a) sea-surface height (normalized with SSH at $t = 0$) and (b) tracer content (normalized with tracer content at $t = 0$).

Tracer evolution of this ring (Fig. 5(a)) shows that filamentation is not much different from the ring in the case of a flat bottom. The ring without bottom friction (Fig. 5(b)) is again subject to less filamentation than with bottom friction turned on. In both cases of bottom friction turned on and off, the decrease in maximum SSH as a function of time (Fig. 3(a)) is larger during the first 60 days in comparison with a flat bottom. After those 60 days, however, the maximum SSH decay is smaller.

The integrated tracer content of the ring as a function of time in the case of a ridge (Fig. 3(b)) is only slightly different from the flat bottom case. After 85 days of the rings evolution with bottom friction on, the ring has the same amount of tracer content, 50%, as in the case of a flat bottom.

In all cases discussed above, a large increase in maximum SSH between days 50–60 occurs which appears to be a result of the boundary conditions we use. A comparison between the (normalized) maximum in SSH with the maxima of relative vorticity, kinetic energy, and potential energy, respectively (Fig. 6), shows that potential energy increases similarly in time as SSH as expected for the barotropic case. A comparison with a model experiment on a larger domain of 1800×1800 km shows a monotonic decay in SSH decay, unlike the 1200×1200 km case, indicating that the domain-size influences the behavior of the barotropic wave (Fig. 7). The barotropic wave energy that is radiated eastward from the ring is not fully absorbed by the sponge layer in the smaller domain. A Kelvin-wave like feature transports the energy clockwise around the basin and influences the ring as soon as it starts to come closer than one Rossby radius of deformation from the western extend of the sponge layer (at day 50). Identical behavior of SSH after 40 days of integration was found by Kamenkovich et al. (1996) in their 2-layer model experiments, but no explanation was given for the local increase of SSH. For the remaining of this paper we analyze the evolution of the ring in the small domain since the dominant terms in the energy balance do not change with increased domain size (see Section 3.3.1).

3.3. *Analysis of 1-layer ring results*

3.3.1. *Energy*

To understand the observed difference in tracer and ring decay described above and the fact that the barotropic ring does not cross the ridge, we look at the evolution of the kinetic energy. The kinetic energy E_{kin} is calculated in three ways: integrated over the ring itself, over the area outside the ring, and over the total domain (Fig. 8(a)). In the case of bottom friction the rate of change of E_{kin} in the ring's interior is dominated by bottom friction and the time-scale of the initial fast decay of the 1-layer ring is determined by the Ekman time-scale of approximately 40 days ($\tau_E = H/f\delta_b$ with δ_b the Ekman layer thickness). However, the energy of the ring is also subject to Rossby-wave radiation which becomes apparent in the case without bottom friction (Fig. 8(b)). Here, we would like to refer to the pioneering works of McWilliams and Flierl (1979), Mied and Lindeman (1979), and Flierl (1984) where Rossby-wave radiation by vortices is first described as well as McDonald (1998) and Flierl and Haines (1994) who all show that Rossby-wave generation leads to radius decay and meridional propagation of eddies.

The energy loss of the ring is approximately 50% after 100 days which is solely due to Rossby-wave radiation as will be demonstrated below. With bottom friction the total energy loss of the ring is as much as 85% in 100 days. It is difficult to separate the energy decay due to bottom friction from that due to Rossby waves since the radiated wave is damped by bottom friction as well.

A periodic pattern with a period of initially 50 and later 70 days is present in both cases, however, more apparent without bottom friction than in the case with bottom friction. To understand its origin we investigate the

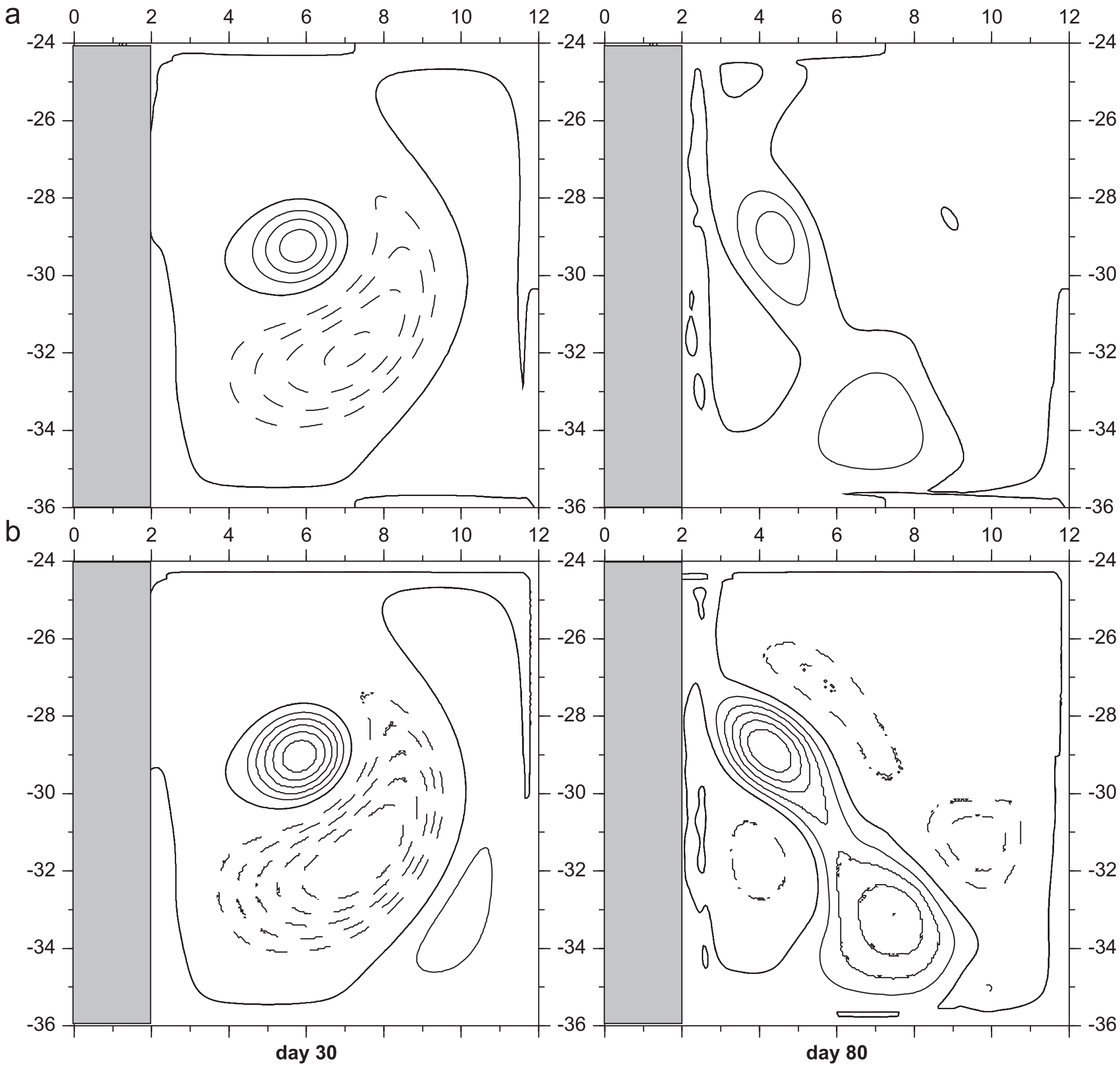

Fig. 4. Sea-surface elevation at days 30 and 80 (contours; interval = 6 cm) for the barotropic ring: (a) ridge with bottom drag and (b) ridge without bottom drag.

contribution of the different terms in the energy equation to the energy budget for the simplest case (1-layer and flat bottom). The equation is obtained by multiplying the barotropic momentum equations with the barotropic velocity $\vec{U}$, and the total depth H, and has the final form

$$H\frac{\partial \frac{1}{2}|\vec{U}|^2}{\partial t} = -\frac{1}{\rho}H\vec{U}\cdot\nabla P_b - H\vec{U}\cdot\nabla\frac{1}{2}|\vec{U}|^2 - Hg\vec{U}\cdot\frac{\partial\vec{\tau}_b}{\partial p} - H\vec{U}\cdot\vec{v_u} \quad (2)$$

where P_b is the barotropic pressure, ρ is the density, $\tau_b = C_d|\bar{u}_b|\bar{u}_b$ is the bottom drag, and v_u is the horizontal turbulent viscosity. The first term on the right-hand side is the pressure work, followed by terms representing advection, dissipation by bottom friction and dissipation by lateral friction. The pressure term can be split up into a potential energy term and an energy flux term. In the 1-layer case, however, the potential energy is two orders of magnitude smaller than the kinetic energy since $g\eta^2/HU^2 \approx L^2/R_d^2 \ll 1$ (using the approximation $L \ll R_d$ and the geostrophic balance $g\eta/L = fU$) and hence, the pressure term is left in this form. Each term is averaged over a period of half a day to average out gravity wave energy (Drijfhout et al., 2003).

Fig. 9(a) shows the local rate of change of kinetic energy ($\partial E_k/\partial t$), (b) the pressure work term, (c) the advective term, and (d) bottom friction for days 10 and 30. These four terms are of similar order of magnitude while lateral friction is negligible.

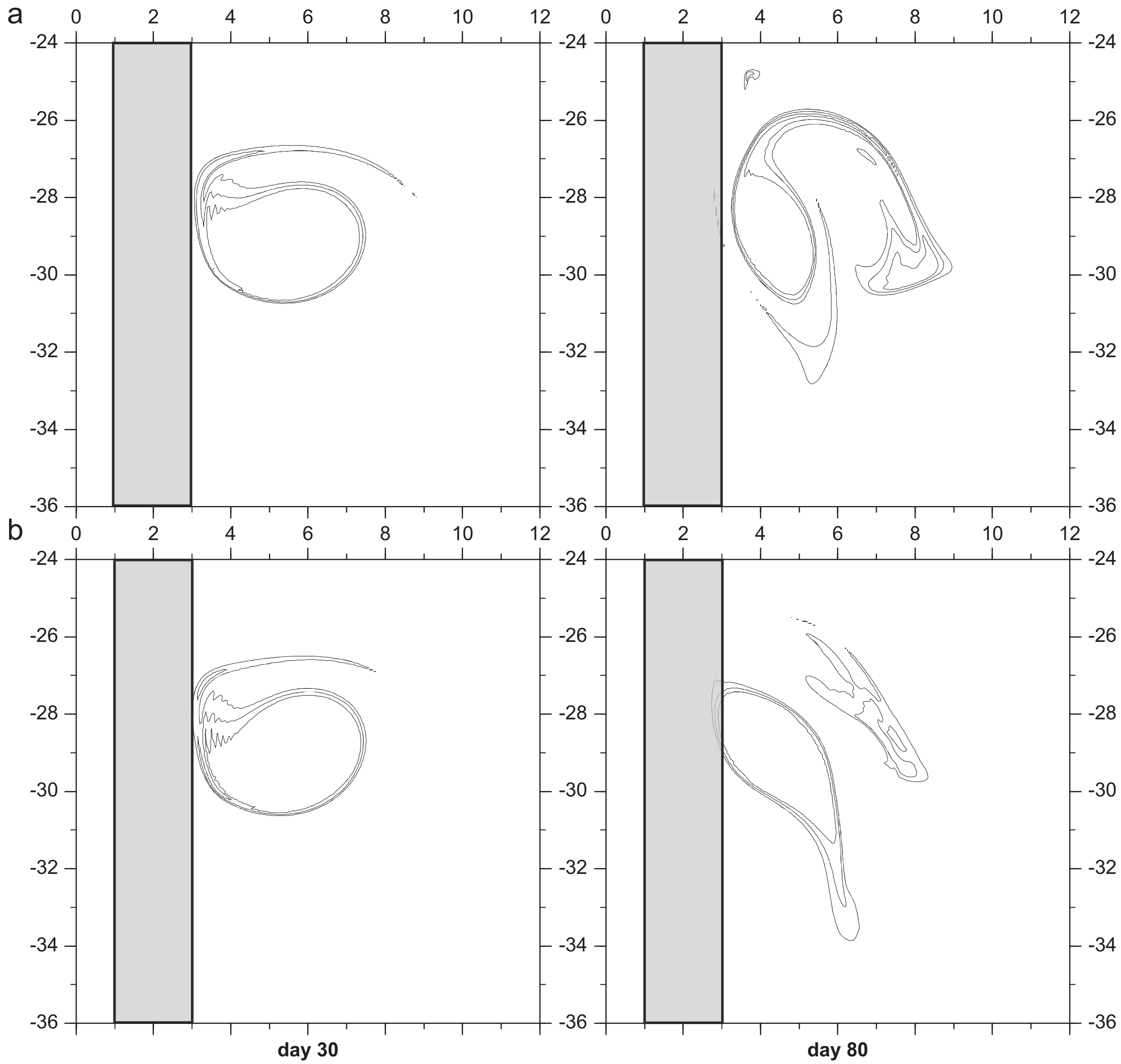

Fig. 5. Tracer concentration at days 30 and 80 (contours; interval = 0.3) for the barotropic ring: (a) ridge with bottom drag and (b) ridge without bottom drag.

At day 10 the ring seems to intensify in its center, which is due to the pressure work term. The pressure work term is governed purely by the ageostrophic flow since $\vec{u} \cdot \nabla P_b$ is zero for geostrophic flow. Since the pressure-gradient force ($-\mathrm{grad}\, p$) is directed outward, the ageostrophic velocity is also directed outward. Hence water is moved from the center to the outer parts of the ring, explaining the fast decay of the maximum SSH in Fig. 3.

The advective term and the bottom friction term are important only in the ring itself. The shape of the advective term is determined by the northwestward motion of the ring center. Both the advective term and the pressure work term show a mode-2 shape after 30 days clearly indicates that a weak barotropic instability has grown from days 10 to 30 and which deforms the ring such that it obtains an elliptical shape. This weak instability is saturated in time since the ring does not split. In the region outside the ring the barotropic Rossby wave is visible in $\partial E_k/\partial t$ and is balanced by the pressure work term. Even though the ageostrophic velocities are still small ($O(1\,\mathrm{cm/s})$) compared to the geostrophic velocities outside the ring ($O(10\,\mathrm{cm/s})$), the pressure work term dominates the evolution of the energy field outside the ring.

When a topographic ridge and bottom friction are present the fields of $\partial E_k/\partial t$, pressure work, advection, and friction are surprisingly identical to the fields for a

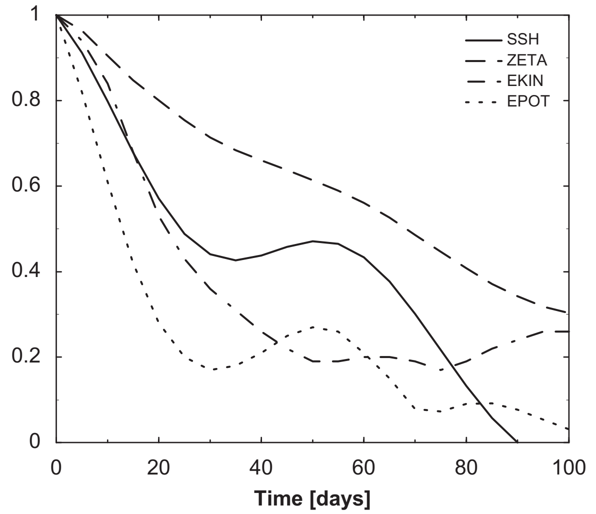

Fig. 6. Maximum of SSH, relative vorticity (ZETA), kinetic energy (EKIN), and potential energy (EPOT) (normalized with SSH at $t = 0$) for the barotropic ring as a function of time. Flat bottom with bottom drag.

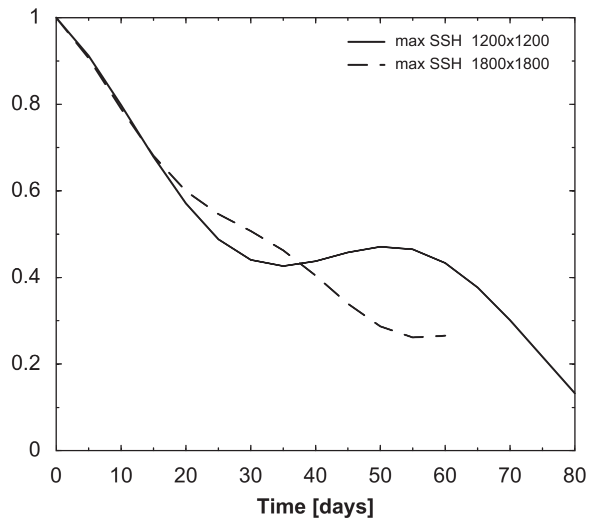

Fig. 7. Maximum of SSH (normalized with SSH at $t = 0$) for two different domain sizes: 1200×1200 km and for 1800×1800 km.

flat bottom (not shown here). We conclude that a topographic ridge has a negligible effect on the energy balance terms of the 1-layer ring but it does prevent the ring from passing.

3.3.2. *The 1-layer vorticity*

We turn to the vorticity balance to study the Rossby-wave decay in more detail. We follow Boudra and Chassignet (1988) and use the full vorticity equation for a primitive-equation model with a generalized vertical coordinate s:

$$\frac{\partial \zeta_s}{\partial t} = -\vec{u}\cdot\nabla_s\zeta_s - \beta v - (\zeta_s + f)\nabla_s\cdot\vec{u} - \vec{k}\cdot\nabla_s\times g\frac{\partial\vec{\tau}_b}{\partial p} + \vec{k}\cdot\nabla_s\times v_u \tag{3}$$

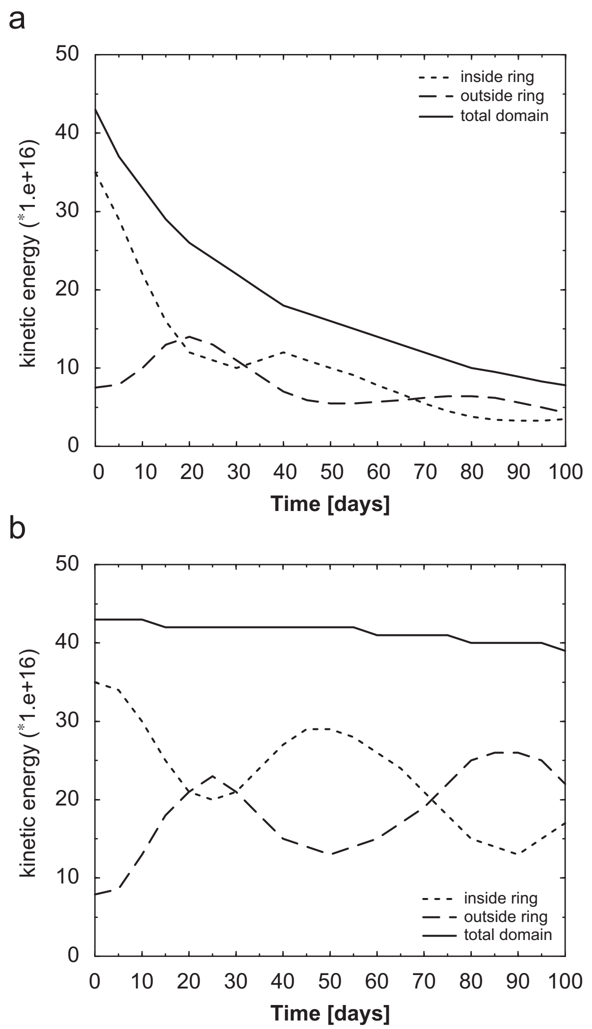

Fig. 8. Kinetic energy for the barotropic ring integrated over different areas: (a) flat bottom with bottom friction and (b) flat bottom without bottom friction.

The vorticity equation consists of relative vorticity advection, planetary vorticity advection, stretching, the curl of bottom friction, and a dissipative term (curl of viscous diffusion). All these terms are averaged over a period of half a day to eliminate the effect of fast gravity waves. The quadratic bottom drag term τ_b is parameterized as $\tau_b = C_d|\bar{u}_b|\bar{u}_b$, where C_d is the drag coefficient and $\bar{u}_b$ represents the average velocity in a slice of water just above the bottom. The horizontal turbulent viscosity is represented by v_u.

For the flat bottom case, the dominant terms in the vorticity equation are the local time derivative of the relative vorticity, ζ_t, the planetary vorticity advection and relative vorticity advection (Fig. 10(a–c), respectively). The stretching term is one order smaller in magnitude since the external Rossby radius of deformation R_d (about a thousand km) is much larger than the ring's radius (about 100 km). The bottom friction and viscous terms are negligible in the vorticity balance. The far field evolution of ζ_t and advection of planetary vorticity

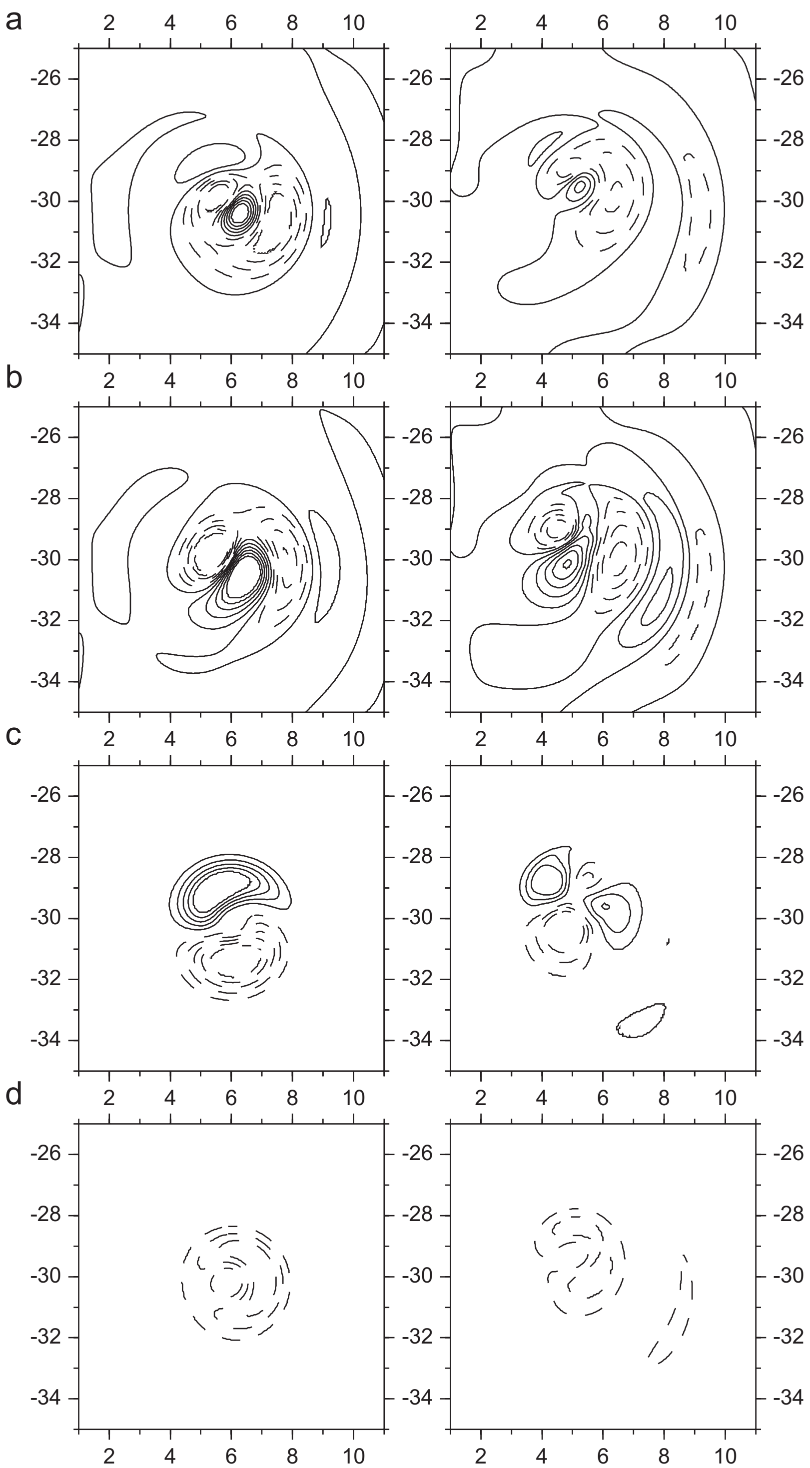

Fig. 9. Energy terms for the barotropic ring, flat bottom: (a) $\partial E_k/\partial t$, (b) pressure work, (c) advection, and (d) bottom friction. For upper three panels: contour interval = 0.3, for lower panel: contour interval = 0.15.

is completely determined by the short Rossby wave ($L \ll R_d$) that is radiated from the ring. In the ring itself ζ_t is determined by the sum of planetary and relative vorticity advection.

The wavelength of the Rossby wave (Fig. 10(b)) is approximately 420 km. Using a phase speed $\beta/k^2 \approx 4\,\mathrm{cm\,s^{-1}}$, the period of the wave is estimated to be 120 days. But, since the ring moves westward at a

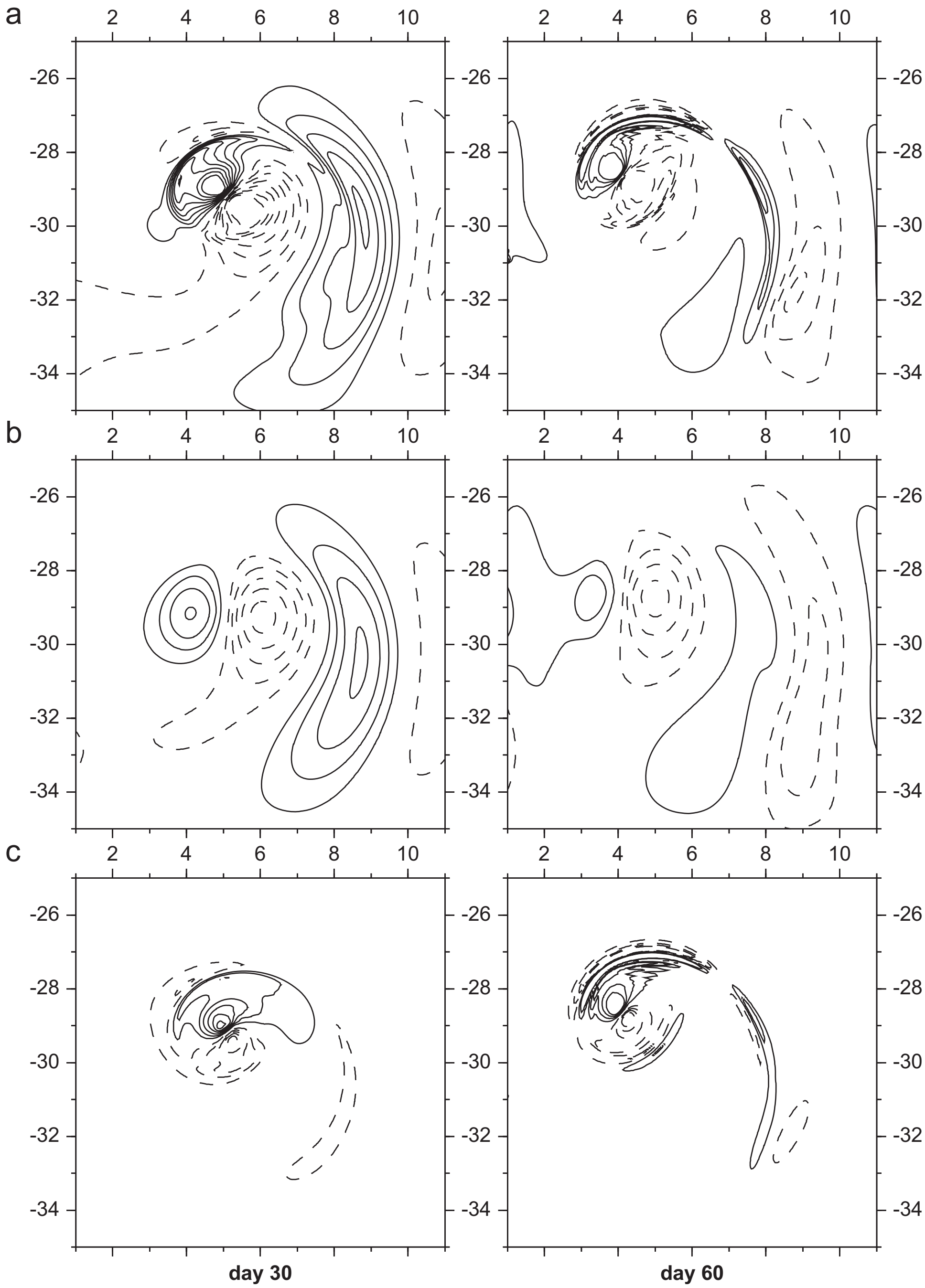

Fig. 10. Vorticity terms for the barotropic ring in case of a flat bottom, at days 30 and 60: (a) $\partial\zeta/\partial t$, (b) planetary vorticity advection, and (c) relative vorticity advection.

speed of $5.5\,\mathrm{km\,day^{-1}} = 6.4\,\mathrm{cm\,s^{-1}}$, the wave energy moves with a speed of $10\,\mathrm{cm\,s^{-1}}$ from the ring. Accordingly, the ring radiates the waves with a 2.5 times higher frequency or 2.5 times smaller period which amounts to $T = 120/2.5 \approx 50$ days, which explains the observed wave period in Fig. 8(b).

Initially, in the case of a ridge, the vorticity balance is identical to the flat bottom case and shows similar Rossby-wave radiation. Bottom friction and lateral dissipation of vorticity are slightly larger along the ridge than in the case of a flat bottom. Due to conservation of potential vorticity, stretching of slope water pulled from the ridge by the outer edges of the ring lead to a patch of negative vorticity as the ring encounters the ridge. This is visible in relative vorticity and advection of relative vorticity in the filament from 29°S, 3°E to 31°S,

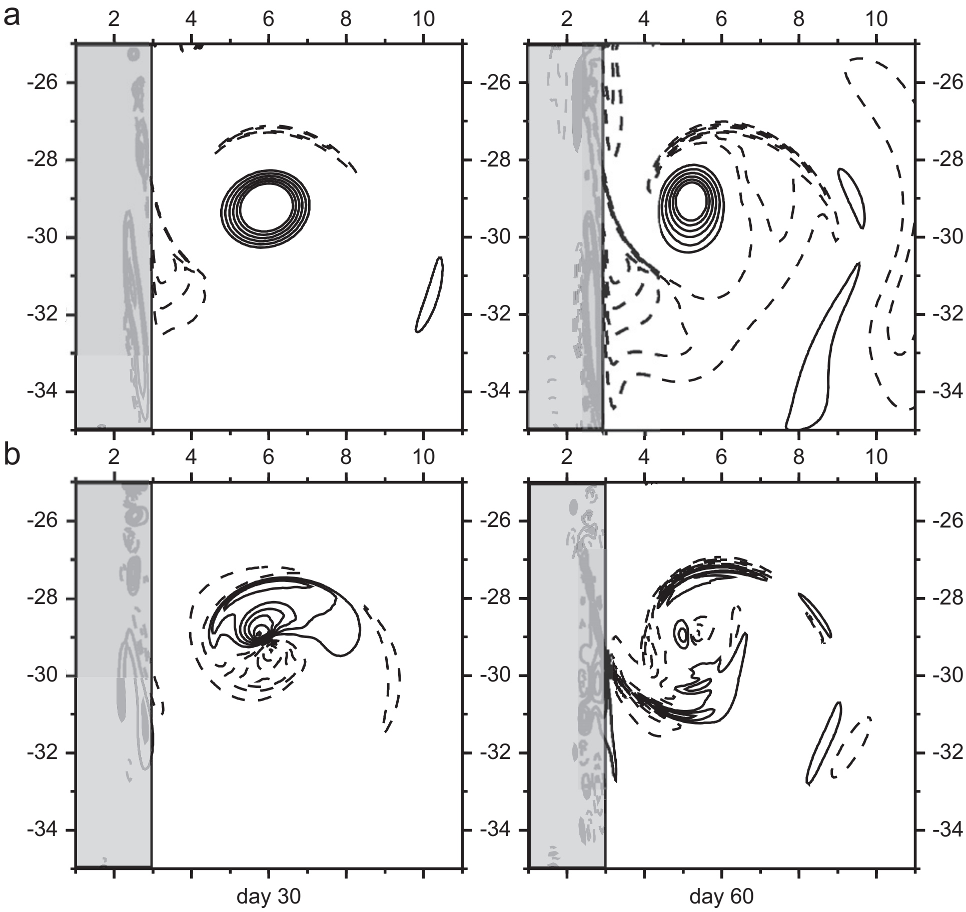

Fig. 11. Relative vorticity for the barotropic ring in case of a ridge, at days 30 and 60: (a) relative vorticity (contour interval $= 0.1 \times 10^{-5}\,\mathrm{s}^{-1}$) and (b) advection of relative vorticity (contour interval $= 0.2 \times 10^{-11}\,\mathrm{s}^{-2}$).

5°E (Fig. 11). This result was previously explained by Zavala Sansón and Van Heijst (2000) and Van Geffen and Davies (2000) and it leads to the dipolar structure visible in SSH (Fig. 4(b)). Once formed, the propagation direction of the dipole is southeastward, preventing the ring from approaching the ridge closer. This can be understood by the following simple order of magnitude argument. The propagation speed of a point vortex pair with circulation strength Γ and distance between the two vortices $2d$ is given by

$$U = \frac{\Gamma}{2\pi 2d} \tag{4}$$

Several experiments with different heights of the ridge show that the ring cannot pass the ridge when it is higher than about 200 m. Potential vorticity conservation of fluid stirred from a ridge of this height leads to a relative vorticity of

$$\zeta = \frac{4000}{3800}f - f = 0.05f \tag{5}$$

leading to a typical circulation strength of $\Gamma \approx 0.05fd^2$. Using now that $f = 10^{-4}\,\mathrm{s}^{-1}$ and $d \approx 200\,\mathrm{km}$ gives a dipole speed of $U \approx 7\,\mathrm{cm/s}$ which is enough to bring the vortex to a halt. Here, the dipole is only well developed in the case without bottom friction. The 1-layer ring with bottom friction dissipates too fast in order to develop this dipolar structure. For a stronger ring (with an initial SSH of 100 cm—not shown here) the dipole does develop completely and southeastward propagation is indeed observed.

4. The 2-layer ring

In this section the influence of a lower layer on the evolution of tracer, energy, and vorticity of a ring approaching a ridge is investigated. The major difference with the barotropic case is that the ring is able to cross the ridge in this case.

4.1. Ring evolution—flat bottom

In all model experiments discussed here bottom friction is included. The ring is initialized at 8°E, 32°S. The time evolution of tracer in the 2-layer ring appears to be very different from the purely barotropic ring (Fig. 12(a)). The ring remains coherent for more than

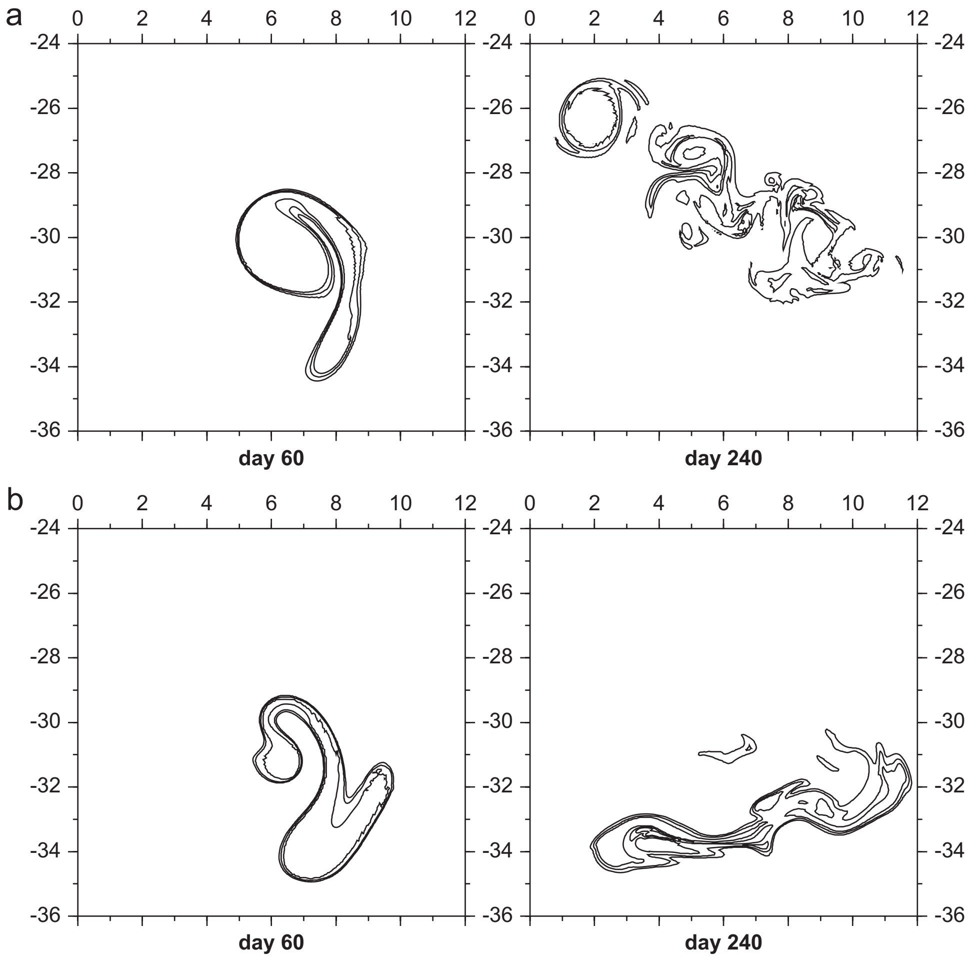

Fig. 12. Tracer concentration (contours; interval = 0.3) at days 60 and 240 for a baroclinic ring with a flat bottom: (a) layer 1 and (b) layer 2.

200 days and it moves at a somewhat slower speed (3.3 km/day) towards the northwest. The tracer filament formed is much larger than for the barotropic case. After 180 days the filament is shed off as a small ring-like structure, which depends on details of the initial velocity profile (Drijfhout et al., 2003). The evolution of tracer in the second layer is very different from that in the upper layer (Fig. 12(b)). There is no tracer left in the lower layer ring at day 240, which corresponds with results from De Steur et al. (2004) where it is shown that for all modeled multi-layer Agulhas rings tracer is completely removed in the layers below the thermocline.

The SSH of the ring decays much slower than in the barotropic case (Fig. 13(a)). After 240 days the SSH has decreased by only 32%. Clearly, in this case the decay time-scale is not determined by bottom friction. The total tracer content in the 2-layer ring as a function of time is determined by the boundary $B = h_1^0 + 5\%(h_1^{max} - h_1^0)$, where h_1^0 is the undisturbed layer thickness of layer 1 and h_1^{max} the maximum layer thickness. The boundary contains the ring and the developing filament as well as the small ring that is shed off at a later stage. The loss of tracer in the upper layer is 60% after 240 days, while all tracer is removed from the lower layer of the ring after 180 days.

4.2. Ring evolution—ridge

In the presence of a topographic ridge, located at 4°E, the initial evolution of tracer in the ring is identical to the case of a flat bottom and shows the same amount of filamentation at day 60 (Fig. 14). Thereafter the ring evolutions become different. At day 240 the filaments that are shed from the ring show a more coherent structure at 5°E, 30°S than in the case of a flat bottom. Also, the filaments remain closer to the ring and are not transported as far to the east as in the case of a flat bottom. The ring propagates in a slightly more westward direction after 180 days when the ring crosses the ridge. During the complete evolution the average speed of the ring is smaller (2.9 km/day) than without the ridge. After 240 days the ring leaves the ridge again on the western side.

The decay of SSH is smaller, only 24% in 240 days, than in the case of a flat bottom. This difference occurs

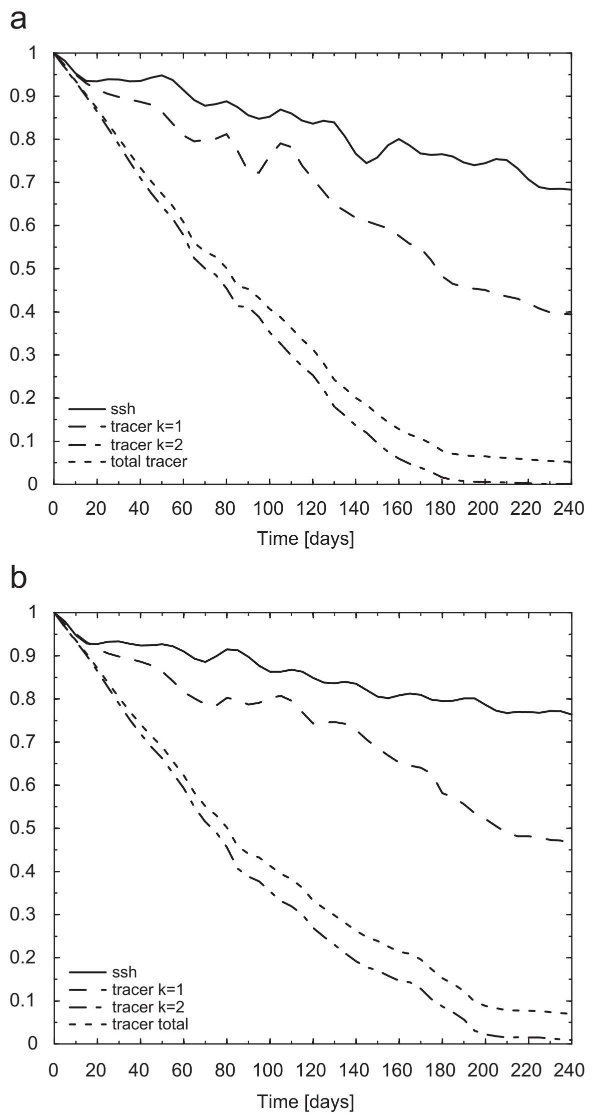

Fig. 13. Maximum sea-surface height and tracer decay for the baroclinic ring as a function of time: (a) flat bottom and (b) ridge ($k=$ layer number).

mainly during the last 100 days of the evolution (Fig. 13). The tracer leakage in both layers is also somewhat less, about 55% in layer 1 while in the lower layer there is still tracer inside the filament after 180 days. Tracer in the lower layer does not cross the ridge, similar to the barotropic case: a coherent structure cannot cross a steep ridge because the potential energy changes needed are much larger than the total energy available.

To summarize, the presence of a ridge has a small effect on the propagation on the ring and is responsible for less loss of tracer and less SSH decay. These results agree with previous findings of Kamenkovich et al. (1996). In the following section a detailed energy and vorticity analysis is given in order to understand this.

4.3. Analysis 2-layer ring results

4.3.1. Energy

We start the analysis with a discussion of the energetics of the ring.

In Fig. 15 the evolution of barotropic kinetic, potential, and total energy are shown, together with the time-integrated lateral and bottom friction terms for the flat bottom case. (The definition of APE we used is $\int\frac{1}{2}\rho_1 g\eta^2\,\mathrm{d}A+\int\frac{1}{2}\rho_2 g'\xi^2\,\mathrm{d}A$. We neglected the linear term $\int\frac{1}{2}\rho_2 g'(h\xi)$, where h is the undisturbed layer thickness of the top layer, which arises in the derivation of APE integrated over the ring and which is dependent on the choice of a reference level. When the linear term in the APE equation is integrated over the total domain, it is equal to zero. Integrated over the ring it is not but we neglect this term since the reference level is, in fact, arbitrary.) The potential energy follows the total energy, which decreases due to bottom friction. The level of kinetic energy remains the same, showing that a constant conversion of potential to kinetic energy takes place, which dissipates at a nearly constant rate. The situation is different outside the ring (Fig. 15(c)). The potential energy decreases at a constant rate, but the kinetic and the total energy increase outside the ring and oscillate with a period of roughly 70 days. Since the kinetic energy sometimes exceeds the potential energy, the presence of barotropic Rossby waves is suggested. We will come back to this later.

Bottom friction is responsible for the overall energy loss, but is not the dominant term inside the ring. Inside the ring (Fig. 15(b)) the total energy loss of the ring is 40% in 240 days. From this figure the total amount of energy dissipated by the bottom friction is estimated to be approximately 25% of the total energy loss of the ring, implying that 10% of the ring energy is dissipated by bottom friction. The remaining 30% of energy loss must be due to radiation of Rossby waves, or due to the shedding of filaments.

A further analysis of the ring evolution is provided by the barotropic kinetic energy equation, which is the barotropic momentum equation multiplied by $\vec{U}H$, where $\vec{U}$is the barotropic velocity and H the total depth. The local rate of change in barotropic kinetic energy $\partial E_k/\partial t$ is given by

$$H\frac{\partial\frac{1}{2}|\vec{U}|^2}{\partial t} = -H\vec{U}\overline{\nabla M} - H\vec{U}\cdot\nabla\frac{1}{2}|\vec{U}|^2 - H\vec{U}\overline{\vec{u}\cdot\nabla\vec{u}} - Hg\vec{U}\cdot\frac{\tau_b}{\partial p} - H\vec{U}\cdot\overline{\vec{v_u}} \tag{6}$$

M is the total Montgomery potential $(M=p+\rho gz)$ and $\vec{u}$ is the total velocity in one layer. $\overline{\nabla M}$ denotes the vertically integrated gradient of the Montgomery potential. Despite the splitting of baroclinic and barotropic pressure fields as is the case in MICOM, we use the total Montgomery potential here, since this is the physical pressure term that determines the barotropic pressure work related with the ageostrophic flow. This total integrated term is called pressure term for short in this section. The third term on the right-hand side denotes

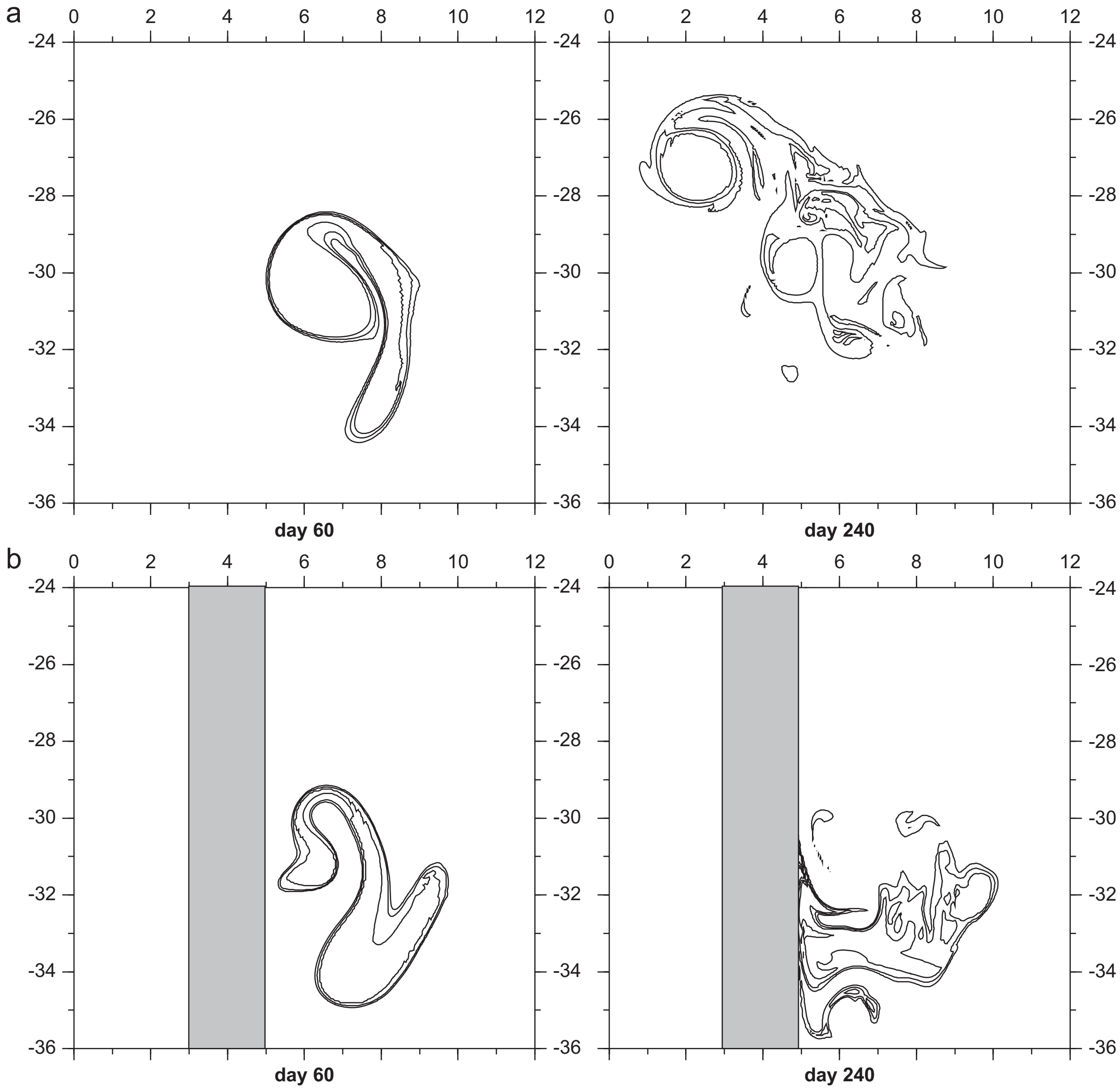

Fig. 14. Tracer concentration (contour interval = 0.3) at days 60 and 240 for a baroclinic ring with a ridge: (a) layer 1 and (b) layer 2.

the barotropic/baroclinic interaction term that describes conversions of baroclinic to barotropic kinetic energy, and vice versa. $\overrightarrow{v_u}$ denotes the vertically integrated dissipative terms.

Fig. 16 shows the spatial distribution of the dominant terms in the barotropic kinetic energy equation at days 80 and 180 in the case of a flat bottom. $\partial E_k/\partial t$ is dominant within the ring at day 80 and is significant in the filament at day 180 (Fig. 16(a)). The barotropic advection term is of the same order of magnitude as $\partial E_k/\partial t$ (Fig. 16(d)), suggesting that to first order barotropic kinetic energy is just advected with the barotropic flow. The filament that is shed from the southeastern side of the ring appears only in $\partial E_k/\partial t$ and the barotropic advective term. Rossby waves are visible in the first 60 days but the order of magnitude is much smaller than the signal of $\partial E_k/\partial t$ in the ring around day 80. This is different from the 1-layer ring where Rossby-wave radiation dominates the energy balance.

The pressure work and barotropic/baroclinic cross terms, terms 1 and 3 on the right-hand side of Eq. (6) (Fig. 16(b) and (c), respectively), are one order of magnitude smaller than the previous two terms and are only visible inside the ring. Interestingly, they seem to counteract each other on both days. In both the barotropic/baroclinic cross terms as well as in the barotropic advective terms there is a clear mode-2 signal present at day 80. This appears due to the fact that the ring has

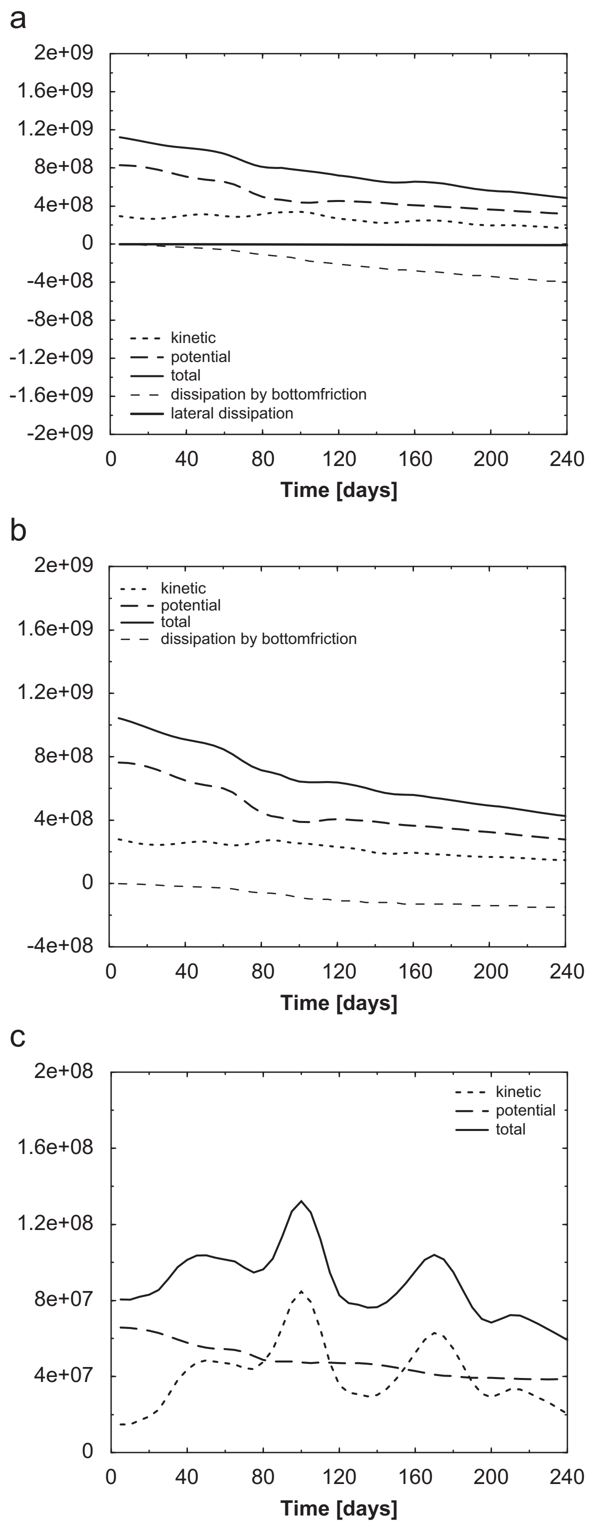

Fig. 15. Kinetic, potential, and total energy for the baroclinic ring with a flat bottom as a function of time: (a) integrated over total domain, (b) inside ring, and (c) outside ring.

become elliptic and is precessing, however, it could also indicate the presence of a weak mixed baroclinic–barotropic instability from days 40 to 120, which is stabilized after the ring has shed the large filament at day 140. Even though the barotropic/baroclinic cross terms are of one order magnitude smaller than $\partial E_k/\partial t$ and barotropic advection, the cross terms are present in the filament (but not visible on the dominant energy scale) which implies that energy conversions take place there too. A further indication that the ring is unstable to an $m = 2$ perturbation is that Drijfhout et al. (2003) have found this instability for ring parameters similar to what is used in this study. See also Katsman et al. (2003).

In the case of a ridge (see Fig. 17), the initial evolution of the energy terms is identical to the flat bottom case, however, the instability is weaker at day 80. After 180 days, when the ring is located on top of the ridge, the energy balance is completely different from the flat bottom case. The mode-2 pattern for the pressure term and cross advective term are now present at day 180, which indicates that enhanced energy conversions occur as the ring crosses the ridge. Analyzing this further, we find that the fluid columns that move uphill give rise to a conversion of baroclinic to barotropic kinetic energy, while descending columns show the reverse which can be understood better if we integrate these energy terms over the ring (Fig. 18(a) and (b)). For the flat bottom, the maxima in $\partial E_k/\partial t$ are determined by the barotropic advection of baroclinic kinetic energy. This implies that the baroclinic kinetic energy is converted into barotropic kinetic energy, which has a maximum after 75 days. After 120 days the energy conversions stabilize. The value of $\partial E_k/\partial t$ shows 2 peaks, one at day 35 and one at day 75, which are to be related with the growth of the mode-2 instability. The modulation of the conversion is related to the position of the $m = 2$ pattern relative to the main filament that is attached to the ring at its northern site. This $m = 2$ pattern has a rotation period of about 100 days, so that the $m = 2$ pattern and the filament have the same orientation relative to each other roughly after 50 days. It is not, however, within the scope of this paper to investigate the possible different growth rates of the instabilities that arise. Our results are in agreement with Katsman et al. (2003) who showed with a linear stability analysis that for a corotating ring the most unstable barotropic mode obtains its energy from the vertical shear.

In the case of a ridge the peak of $\partial E_k/\partial t$ at day 75 is smaller compared to the flat bottom case which indicates that conversion from baroclinic to barotropic kinetic energy is less (Fig. 18(b)). As the edge of the ring touches the ridge around day 60, the steep topography inhibits the development of the $m = 2$ instability. But between days 120 and 200, as the ring passes the ridge, enhanced baroclinic/barotropic conversions in the ring take place. The barotropic kinetic energy increases during the ascent of the ridge, to decrease strongly during the descent of the ridge.

Associated with this one must realize that the 2-layer ring is not purely co-rotating anymore. Already in the case of a flat bottom, the lower layer velocities indicate the presence of a hetonic structure (Hogg and Stommel, 1985; Matano and Beier, 2003) where a lower-layer cyclone forms a dipole structure with the upper-layer anticyclone.

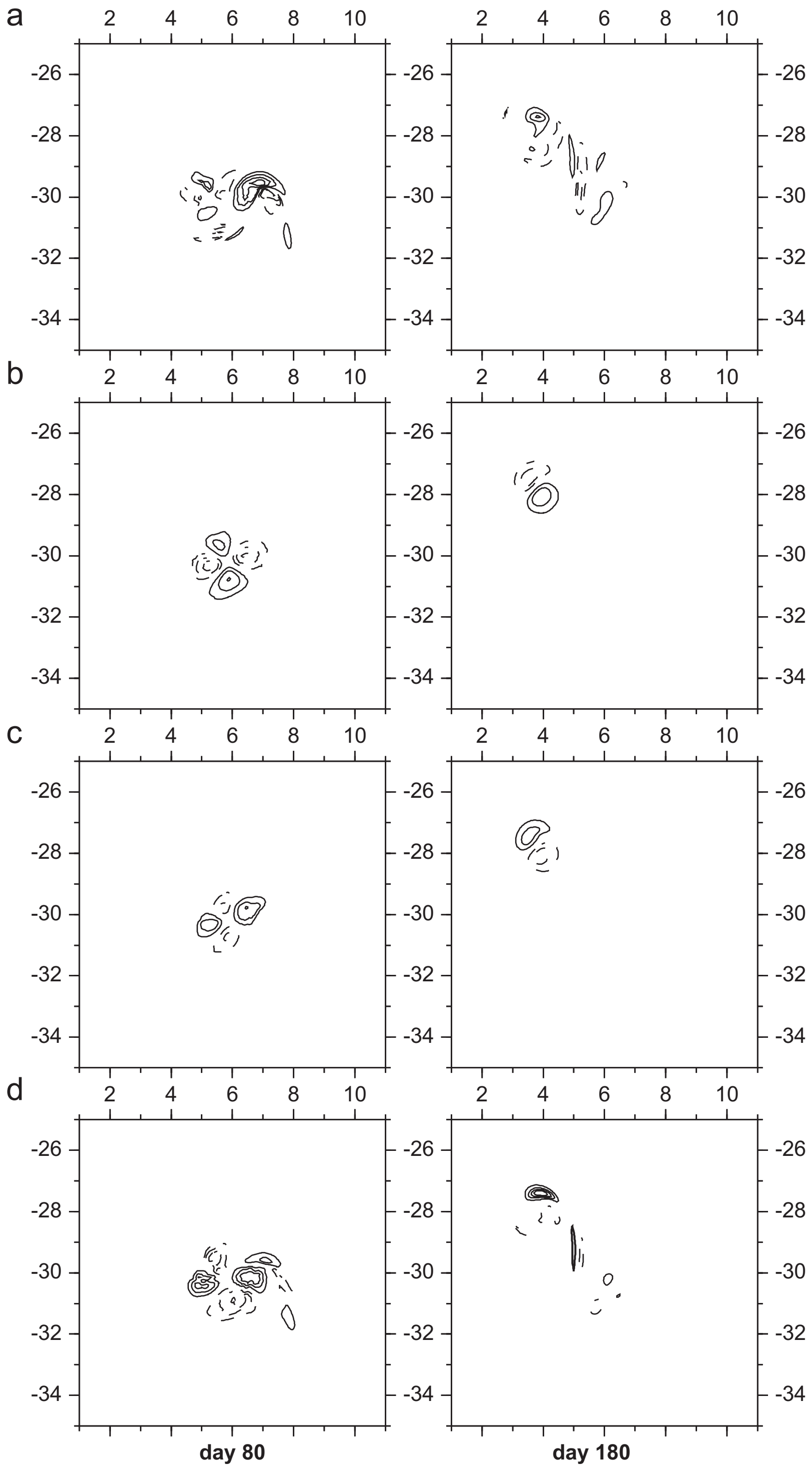

Fig. 16. Energy terms for the baroclinic ring, flat bottom: (a) $\partial E_k/\partial t$ (contour interval $= 0.6 \times 10^{-5}$ and 0.2×10^{-5} resp.), (b) pressure work (contour interval $= 0.2 \times 10^{-6}$ and 0.1×10^{-6} resp.), (c) cross advection (contour interval $= 0.2 \times 10^{-6}$ and 0.1×10^{-6} resp.), and (d) barotropic advection (contour interval $= 0.6 \times 10^{-5}$ and 0.2×10^{-5} resp.).

The axis of the pair is tilted with respect to the vertical (with the cyclone lagging the anticyclone). This structure develops in all the rings described here after approximately after 20 days.

During the ascent of the ridge the lower-layer velocities must decrease to avoid too large potential energy changes (see the barotropic case for a more thorough description of this effect). This means that the

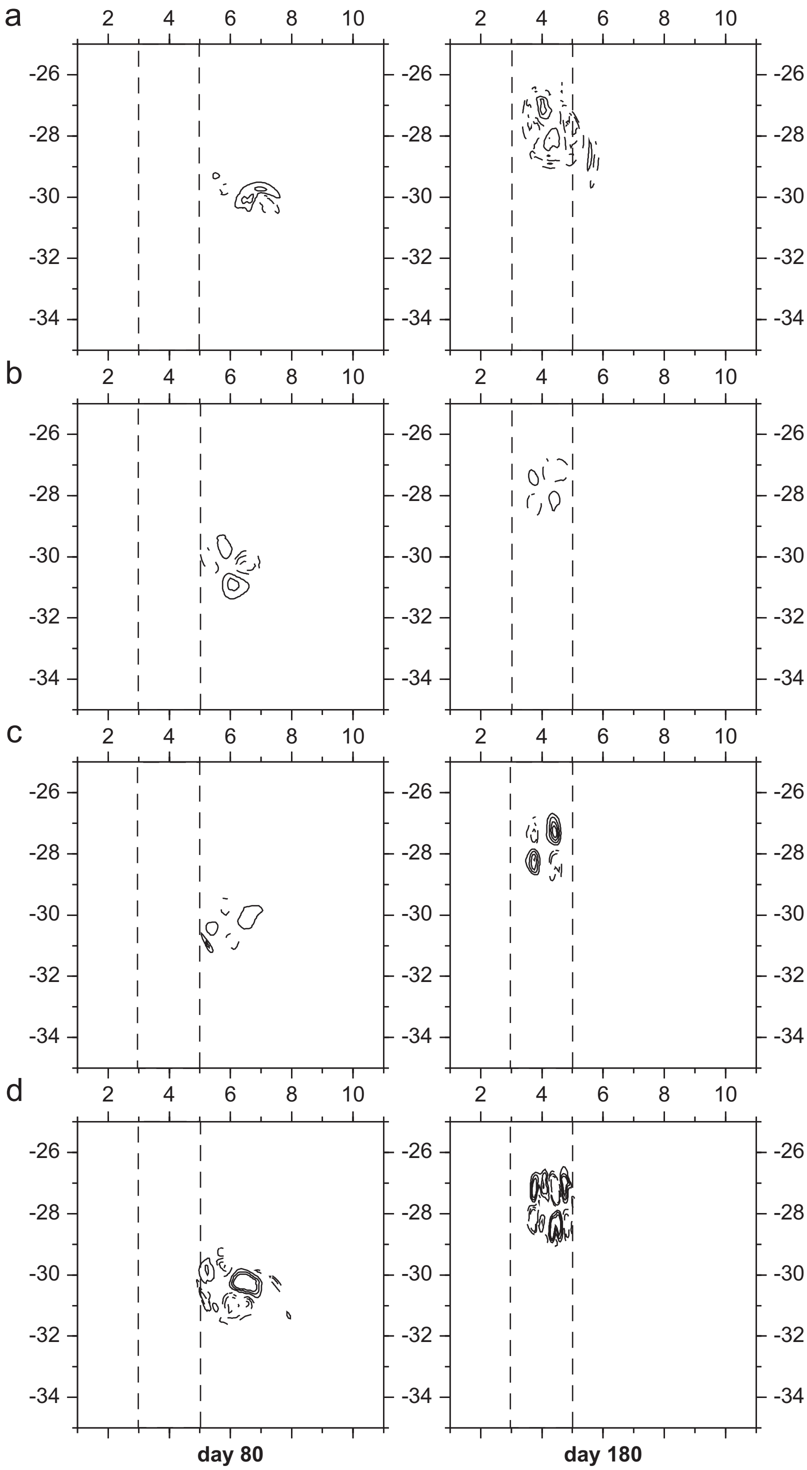

Fig. 17. Energy terms for the baroclinic ring in the case of a ridge: (a) $\partial E_k/\partial t$ (contour interval = 0.8×10^{-5} and 0.4×10^{-5} resp.), (b) pressure work (contour interval = 0.2×10^{-6} and 0.2×10^{-6} resp.), (c) cross advection (contour interval = 0.2×10^{-6} and 0.2×10^{-6} resp.), and (d) barotropic advection (contour interval = 0.8×10^{-5} and 0.8×10^{-5} resp.).

lower-layer cyclonic motion reduces, leading to an increase of the vertically averaged anticyclonic rotation and hence a larger barotropic kinetic energy. The reverse process happens during ridge descent.

We are now in the position to understand part of the reason why the SSH decay is smaller when a ridge is present: as soon as the ring encounters the ridge kinetic energy is transferred from lower to upper

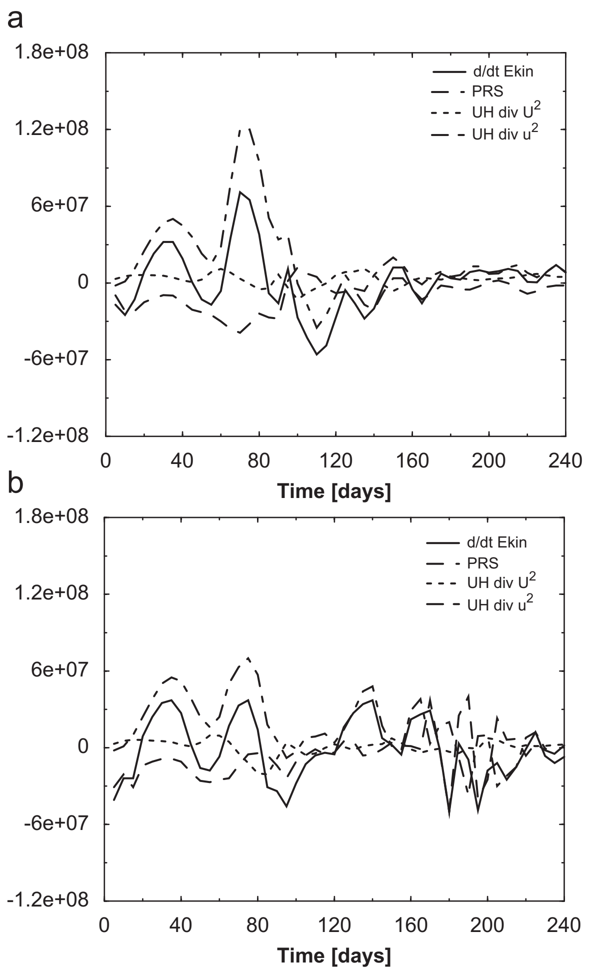

Fig. 18. Energy terms integrated over the baroclinic ring as a function of time: (a) flat bottom and (b) ridge.

layer, which by geostrophy gives rise to a higher SSH. Also the barotropic kinetic energy increases, which will tend to increase the SSH further. Furthermore, the SSH decay related with the $m = 2$ instability is suppressed due to geometric constraints. Because bottom friction is always present an overall decrease in SSH is present, but the decay of SSH is less (Fig. 12(b)). However, this is not the full story. Rossby-wave radiation of the rings energy should also be taken into account as shown with the vorticity balance in the following subsection.

4.3.2. Vorticity

The vorticity balance as shown in Eq. (3) is calculated for each layer and is shown for the flat-bottom case (Fig. 19(a–d)). In the 2-layer case $\partial\zeta_s/\partial t$ in the upper layer is to be first order determined by advection of relative vorticity, followed by advection of planetary vorticity and the stretching term. At day 180 (in fact already after 120 days) many small-scale vorticity filaments are visible in the wake of the ring. Advection of planetary vorticity and the stretching term are important only in the ring itself. The stretching term shows a clear mode-2 structure from days 60 to 120. On the dominant scales there are no Rossby waves visible in the upper layer.

In the lower layer the vorticity terms are one order smaller than in the upper layer (Fig. 20). Again, relative vorticity advection balances $\partial\zeta_s/\partial t$ in the ring, in the filament, and finally in small-scale structures in the wake of the ring. The main difference from the upper layer is the presence of Rossby-wave radiation in the term representing advection of planetary vorticity which is similar to what Flierl (1984) found though more nonlinear.

Advection of planetary vorticity balances with $\partial\zeta_s/\partial t$ in the Rossby waves which indicates the barotropic nature of the waves. The effect of Rossby-wave radiation is only visible in lowest layer since the rotational velocities are small here. The difference in the vorticity balance in the two layers indicates that different physical mechanisms play a role in the two layers. In the top layer the nonlinearity of the ring is too large for the Rossby waves to have an significant impact on the decay of the ring. There, vorticity is removed from the ring by advection of relative vorticity, mainly through small filaments. In the lower layer, Rossby waves couple with the ring and change the vorticity field of the ring.

This view is confirmed by the spatial structure of relative vorticity. Relative vorticity for the 2-layer ring is shown for the top layer (Fig. 21(a)) and the lower layer (Fig. 21(b)). (These fields might look noisy, but do recall that the resolution is very low, only 5 km.)

At day 60 the relative vorticity in both layers is of the same sign for most regions in the waves, confirming their barotropic nature. In the upper layer the ring structure remains visible until day 240 while in the lower layer the rings structure does not remain coherent at all. This is consistent with the findings of De Steur et al. (2004), who showed that the lower layers dynamics is governed by Rossby-wave radiation since the rotational velocities in the lower layer are much smaller than in the upper layer and the initial vorticity anomaly can be radiated away by Rossby waves.

When a ridge is present, the dominating terms in the vorticity balance in the upper layer are the same as for the flat bottom (not shown). The main difference occurs at day 180 when the ring shows interaction with the ridge, visible in the stretching term (Fig. 22(a)). The ascending fluid columns increase the barotropic relative vorticity, while descending fluid columns decrease it. This is consistent with what we have found for the energy conversion terms. In the lower layer advection of planetary vorticity shows radiation of Rossby waves until day 180, when the eastern edge of the ring starts to ascend the ridge (Fig. 22(b)). At day 240, when the ring has passed the ridge, radiation from the ring stagnates and the Rossby waves decay on the eastern side of the ridge. As in the 1-layer case, barotropic flow cannot cross the steep ridge, hence, the barotropic Rossby-wave generation comes to a halt, resulting in less decay of barotropic energy of the ring and less SSH decay.

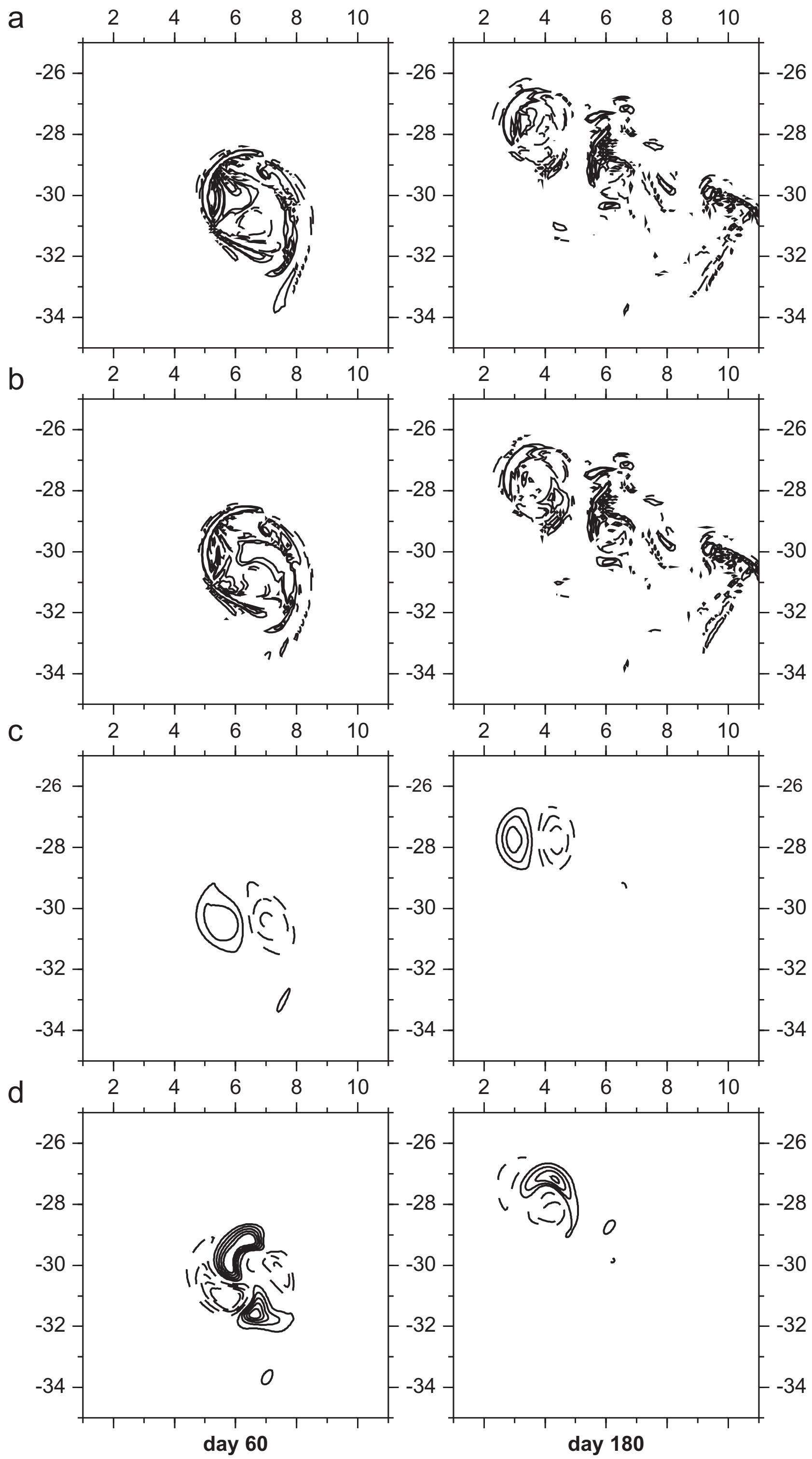

Fig. 19. Vorticity terms ($\times 10^{-11}$) in layer 1 of the baroclinic ring with a flat bottom, at days 60 and 180: (a) $\partial\zeta/\partial t$ (contour interval $= 0.8\,s^{-2}$), (b) relative vorticity advection (contour interval $= 0.8\,s^{-2}$), (c) planetary vorticity advection (contour interval $= 0.4\,s^{-2}$), and (d) stretching (contour interval $= 0.4\,s^{-2}$).

5. Conclusions and discussion

The decay of an Agulhas ring in presence of a ridge has been investigated in a one and a two-layer version of the MICOM model. Several experiments have been performed, and we report here on two of these in detail to understand the mechanisms that determine the decay with and without a ridge.

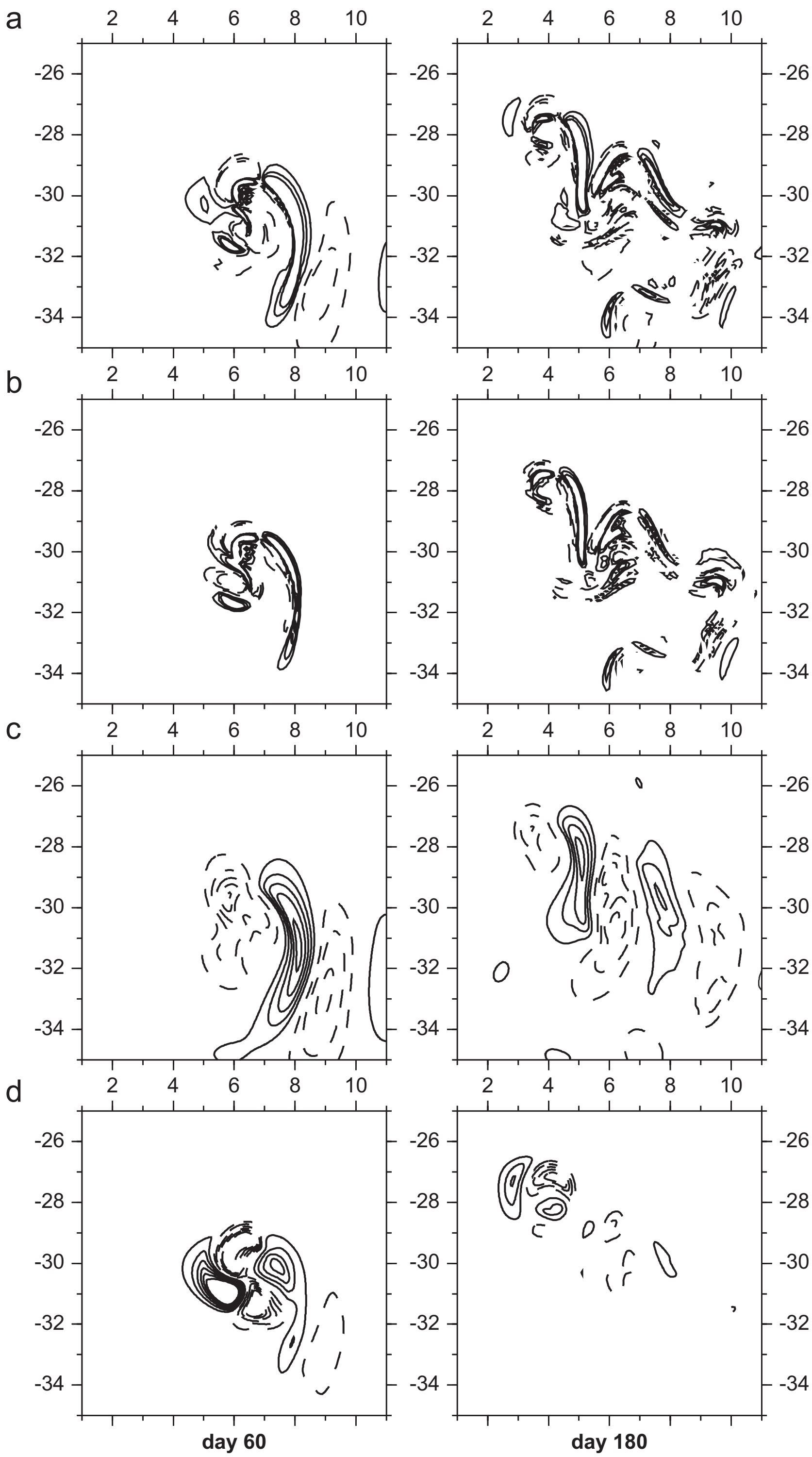

Fig. 20. Vorticity terms ($\times 10^{-12}$) in layer 2 of the baroclinic ring with a flat bottom, at days 60 and 180: (a) $\partial\zeta/\partial t$ (contour interval = 1 s^{-2}), (b) relative vorticity advection (contour interval = 1 s^{-2}), (c) planetary vorticity advection (contour interval = 0.5 s^{-2}), and (d) stretching (contour interval = 0.5 s^{-2}).

For a 1-layer ring with bottom friction, the initial fast decay of SSH is dominated by the Ekman time-scale of about 40 days, which is shown by the dominance of bottom friction term in the barotropic energy balance. Thereafter, SSH decays further by radiation of barotropic Rossby waves until the ring reaches the

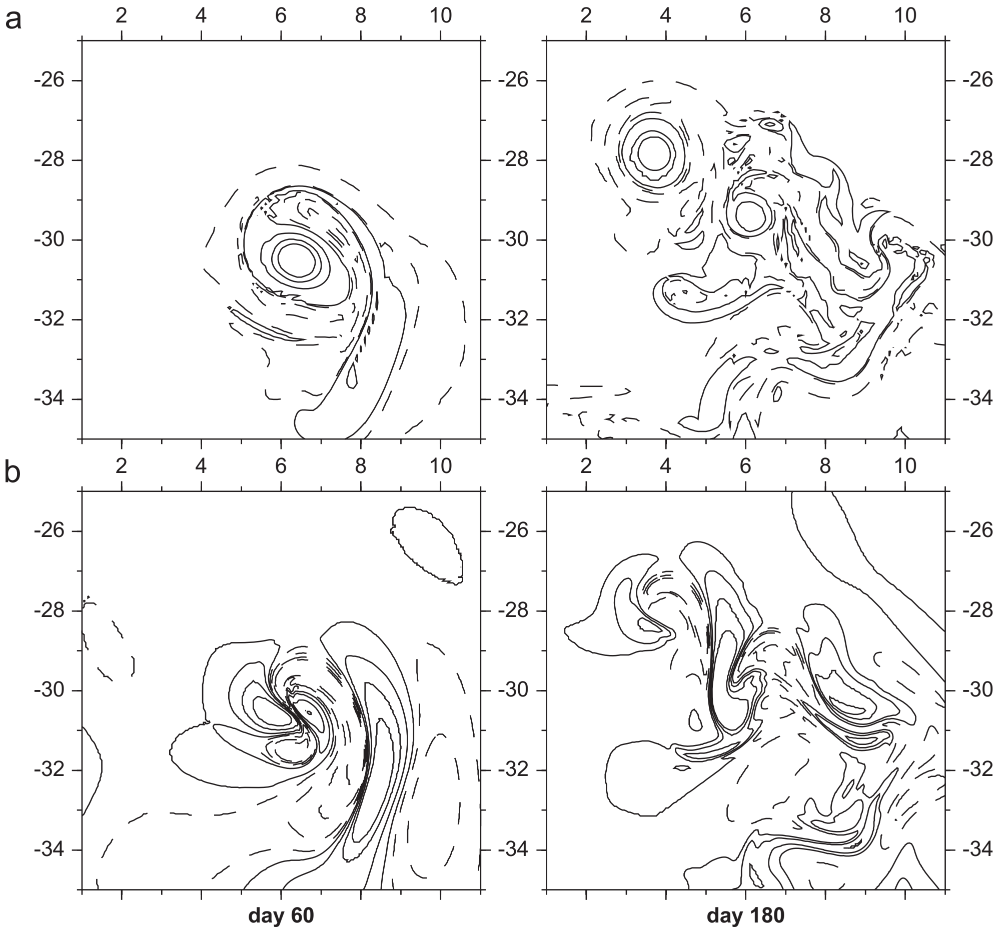

Fig. 21. Relative vorticity ($0.7\times10^{-5}\,\mathrm{s}^{-1}$), baroclinic ring, flat bottom, at days 60 and 180: (a) layer 1 and (b) layer 2.

boundary. When bottom friction is not present, the initial decay of SSH still shows a decrease, being less, however, than in the case with bottom friction. This means that during the initial stage radiation of Rossby waves is responsible for the loss of energy from the ring, which accounts for almost half of the energy loss of the ring in 100 days. The 1-layer ring cannot cross the ridge as a coherent structure because the ascending fluid patch would lead to an enormous increase in potential energy which is much larger than the total energy available. Furthermore, stirring of water from the slope by the outer edges of the ring lead to the formation of a patch of negative relative vorticity, which, together with the positive relative vorticity of the ring forms a dipole, which propagates southeastward, away from the ridge.

In a two-layer ocean, the tracer decay in the upper layer is much less due to the more coherent structure of the ring. In the lower layer the tracer decay is substantial because the lower-layer swirling velocities are smaller than the propagation speed of the ring, so that lower-layer fluid is not trapped in the ring (Flierl, 1981). This is related to the size of the so-called separatrix that separates trapped ring-water from the surroundings of the ring (De Steur et al., 2004). In presence of a ridge, the propagation speed of the ring reduces slightly, leading to a larger area of trapped fluid in the upper layer, so less tracer loss. The leakage in the lower layer is also affected by the slowing down of the ring, since there is still tracer present in the lower layer of the ring around 180 days, while in the case of a flat bottom all the tracer is stirred from the lower layer ring at that point. (Note that the decreased tracer leakage is not directly related to the decrease in Rossby-wave radiation, since linear Rossby waves do not carry tracer.)

The SSH decay of the 2-layer ring with a flat bottom is almost linear but shows less decay when the ring encounters the topographic ridge. In the flat bottom case the SSH decay is dominantly associated with the instability and associated energy conversions of the ring, together with the formation of a large filament that detaches from the ring. In the lower layer radiation of barotropic Rossby waves and bottom friction are dominant.

All rings investigated still possess an $m=2$ instability which could not be removed by introducing the approximated stable ring profile that is used by Herbette et al. (2003). Despite the presence of some instability characteristics, the ring does not split into two but develops a large filament that evolves towards a ring-like structure

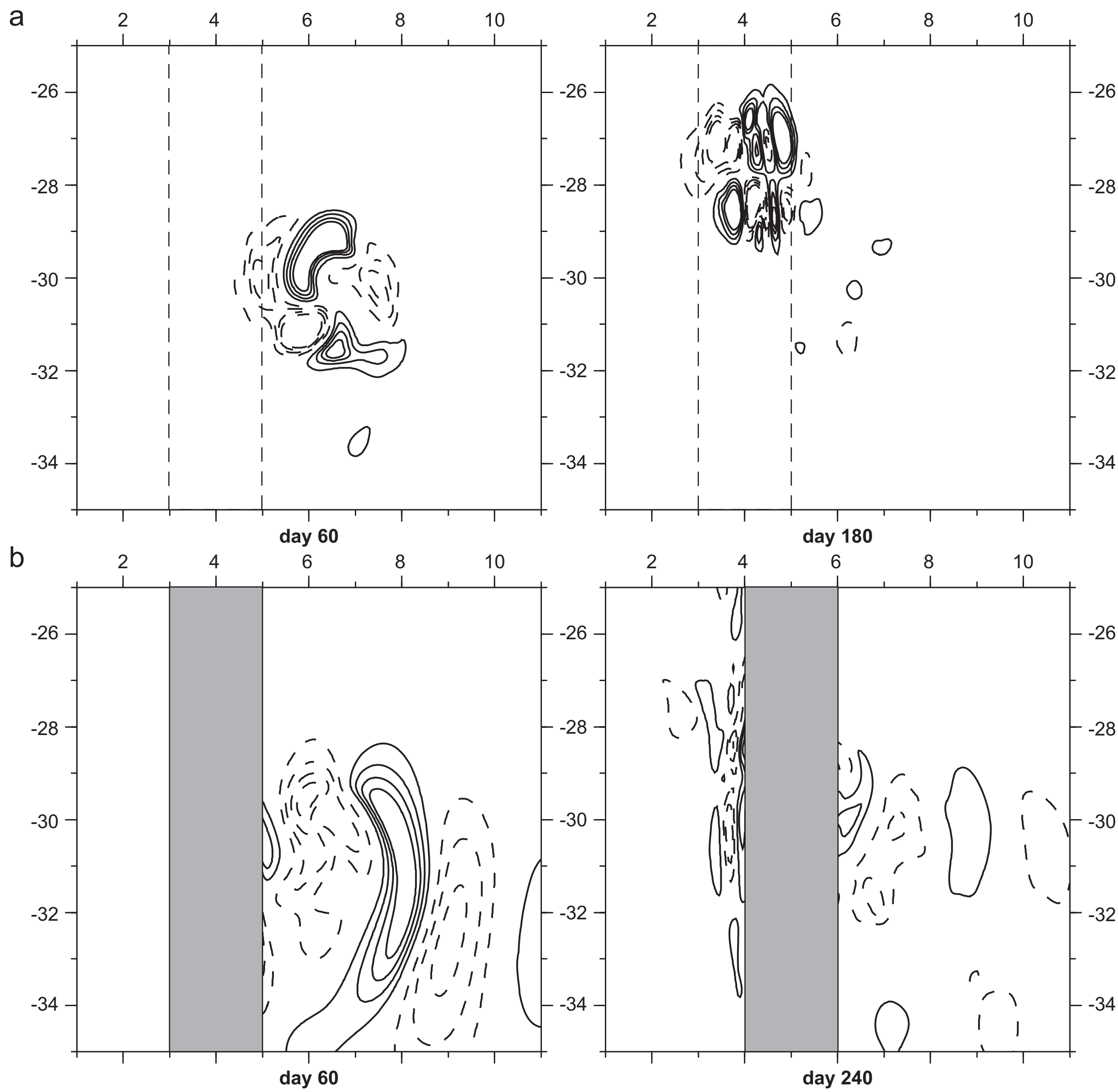

Fig. 22. Vorticity terms in the case of a ridge of the baroclinic ring: (a) stretching term ($\times 10^{-11}$) in layer 1 at days 60 and 180 (contour interval $= 0.4\,s^{-2}$) and (b) planetary vorticity advection ($\times 10^{-12}$) in layer 2 at days 60 and 240 (contour interval $= 0.5\,s^{-2}$).

that also shows the mode-2 instability. The Rossby-wave radiation is smaller than in the barotropic case and has its largest impact on the lowest layer, while the upper layer is less affected due to its large nonlinearity. The total velocity field in the lower layer changes swiftly from co-rotating to an erratic radiating flow field with a many small-scale structures, visible in the relative vorticity of layer 2. Hence, the ring changes largely due to a nonlinear instability and barotropic Rossby-wave radiation.

The nonlinear upper layer of the ring is not completely decoupled from the lower layer since the ring and the associated energy conversion terms show interaction with the ridge. When encountering the ridge, the upper layer ring shows enhanced baroclinic/barotropic energy conversions. These enhance the kinetic barotropic energy of the ring as well as the upper-layer velocities, and so reduce the SSH decay. The barotropic Rossby-wave radiation mainly visible in the lower layer stops when the ring is on the ridge since barotropic signals cannot pass the ridge, as explained above. And, finally, the $m = 2$ instability is inhibited when the ring encounters the ridge due to geometrical constraints. These three mechanisms lead to smaller SSH decay of the ring when a ridge is present.

It is difficult to distinguish the kinetic energy decay related to the $m = 2$ instability and that related to Rossby waves. The instability leads only to energy conversions and not to a net energy loss from the ring while Rossby waves do radiate energy. In previous studies of Drijfhout et al. (2003) and De Steur et al. (2004) it was shown that on the f-plane SSH of the ring decays as well. Hence, the net effect of Rossby waves on the decay of SSH of rings is relatively small compared to the instability. Here, the energy loss by Rossby waves is estimated to be 30% for the baroclinic ring. The effect of bottom friction is substantial in the case of the baroclinic ring and dissipates about 10% of the rings initial energy. The Rossby waves have the largest effect on the rings structure in the lower layer which is exactly needed for the ring to be able to cross topography.

An increase of mixing due to the ridge as was suggested by for instance Byrne et al. (1995) and Schouten et al. (2000) is not in agreement with our findings. We find the same results as Kamenkovich et al. (1996) that rings that encounter a topographic ridge transport more tracer. The tracer loss of the ring that crosses the ridge is 5% less in the case presented here. A large topographic ridge is thus responsible for less stirring of Agulhas water from the ring, which is perhaps quite counter-intuitive. We have not, however, explored the effects or variations of possible small-scale mixing events due to, for instance, internal waves.

In this paper we showed results for a specific ring structure, one for the barotropic and one for a baroclinic ocean. The Agulhas rings present in the Cape Basin are of variable sizes and strengths due to the strong variability in the ring shedding process and due to various splitting and merging events of rings. This implies that not all Agulhas rings have the same strong barotropic component as measured for instance by Van Aken et al. (2003), on which the present analysis was based. We have conducted several experiments with rings of variable spatial structure and size, which showed similar evolutions as the rings presented here. While the more baroclinic rings can cross the ridge more easily we can expect that rings that still have a relatively strong barotropic component while reaching the Walvis Ridge shall be slowed down or be steered along the bathymetry due to vorticity effects until they have adjusted to a less barotropic state. Agulhas rings will cross the ridge once they have reached a compensated state due to nonlinear stabilization and Rossby-wave radiation which is directly related with the observed stagnation of decay of SSH of the rings as they cross the Walvis Ridge.

Acknowledgments

We would like to thank Eric Chassignet for having provided us the numerical code of the vorticity balance for MICOM. We thank Sybren Drijfhout and Sjef Zimmerman for useful discussions and suggestions throughout this study. This research was part of the MARE project and the CLIVARNET program and was funded by the Foundation for Earth and Live sciences (ALW) of the Netherlands Foundation of Scientific Research (NWO) under Grant 750-712.00B. Part of this work was sponsored by the Stichting Nationale Computerfaciliteiten (NCF) for the use of supercomputer facilities.

References

Beismann, J.O., Käse, R.H., Lutjeharms, J.R.E., 1999. On the influence of submarine ridges on translation and stability of Agulhas rings. Journal of Geophysical Research 104 (C4), 7897–7906.
Bleck, R., Smith, L.T., 1990. A wind-driven isopycnic coordinate model of the north and equatorial Atlantic ocean. 1. Model development and supporting experiments. Journal of Geophysical Research 95, 3273–3505.
Boudra, D.B., Chassignet, E.P., 1988. Dynamics of Agulhas retroflection and ring formation in a numerical model. Part 1: the vorticity balance. Journal of Physical Oceanography 18, 280–303.
Byrne, D.A., Gordon, A.L., Haxby, W.F., 1995. Agulhas eddies: a synoptic view using Geosat ERM data. Journal of Physical Oceanography 25, 902–917.
Carton, X., McWilliams, J., 1989. Barotropic and Baroclinic Instabilities of Axisymmetric Vortices in a QG Model. Elsevier, Amsterdam (pp. 225–244).
De Ruijter, W.P.M., Biastoch, A., Drijfhout, S.S., Lutjeharms, J.R.E., Matano, R.P., Pichevin, T., van Leeuwen, P.J., Weijer, W., 1999. Indian–Atlantic interocean exchange: dynamics estimation and impact. Journal of Geophysical Research 104, 20885–20910.
De Steur, L., van Leeuwen, P.J., Drijfhout, S.S., 2004. Tracer leakage from modeled Agulhas rings. Journal of Physical Oceanography 34 (6), 1387–1399.
Drijfhout, S.S., Katsman, C.A., de Steur, L., van der Vaart, P.C.F., van Leeuwen, P.J., Veth, C., 2003. Modeling the initial fast sea-surface height decay of Agulhas ring "Astrid". Deep-Sea Research II 50, 299–319.
Duncombe Rae, C.M., Garzoli, S.L., Gordon, A.L., 1996. The eddy field of the southeast Atlantic ocean: a statistical census from the Benguala sources and transports project. Journal of Geophysical Research 101, 11949–11964.
Flierl, G.R., 1981. Particle motions in large-amplitude wave fields. Geophysical and Astrophysical Fluid Dynamics 18, 39–74.
Flierl, G.R., 1984. Rossby wave radiation from a strongly nonlinear warm eddy. Journal of Physical Oceanography 14, 47–58.
Flierl, G.R., Haines, K., 1994. The decay of modons due to Rossby wave radiation. Physics of Fluids 6, 3487–3497.
Gordon, A.L., 1986. Interocean exchange of thermocline water. Journal of Geophysical Research 91, 5037–5046.
Herbette, S., Morel, Y., Arhan, M., 2003. Erosion of a surface vortex by a seamount. Journal of Physical Oceanography 33, 1664–1679.
Hogg, N.G., Stommel, H.M., 1985. Hetonic explosions: the breakup and spread of warm pools as explained by baroclinic point vortices. Journal of Atmospheric Science 42, 1465–1476.
Jacob, J.P., Chassignet, E.P., Dewar, W.K., 2002. Influence of topography on the propagation of isolated eddies. Journal of Physical Oceanography 2848–2869.
Kamenkovich, V.M., Leonov, Y.P., Nechaev, D.A., Byrne, D.A., Gordon, A.L., 1996. On the influence of bottom topography on the Agulhas eddy. Journal of Physical Oceanography 26, 892–912.
Katsman, C.A., van der Vaart, P.C.F., Dijkstra, H.A., de Ruijter, W.P.M., 2003. Stability of multilayer vortices, a parameter study including realistic Gulf Stream and Agulhas rings. Journal of Physical Oceanography 33, 1197–1218.
Matano, R.P., Beier, E.J., 2003. A kinematic analysis of the Indian–Atlantic interocean exchange. Deep-Sea Research II 50, 229–249.
McDonald, N.R., 1998. The decay of cyclonic eddies by Rossby-wave radiation. Journal of Fluid Mechanics 361, 237–252.
McWilliams, J.C., Flierl, G.R., 1979. On the evolution of isolated, nonlinear vortices. Journal of Physical Oceanography 9, 1155–1182.
Mied, R.P., Lindeman, G.J., 1979. The propagation and evolution of cyclonic Gulf Stream rings. Journal of Physical Oceanography 9, 1183–1206.
Schouten, M.W., de Ruijter, W.P.M., van Leeuwen, P.J., 2000. Translation, decay and splitting of Agulhas rings in the southeastern Atlantic Ocean. Journal of Geophysical Research 105 (C9), 21913–21925.
Smith, D.C., O'Brian, J.J., 1983. The interaction of a two-layer isolated mesoscale eddy with bottom topography. Journal of Physical Oceanography 13, 1681–1697.
Thierry, V., Morel, Y., 1999. Influence of a strong bottom slope on the evolution of a surface-intensified vortex. Journal of Physical Oceanography 911–924.

Van Aken, H.M., Van Veldhoven, A.K., Veth, C., De Ruijter, W.P.M., Van Leeuwen, P.J., Drijfhout, S.S., Whittle, C.P., Rouault, M., 2003. Observations of a young Agulhas ring, Astrid, during MARE in March 2000. Deep-Sea Research II 50, 167–195.
Van Ballegooyen, R.C., Gründlingh, M.L., Lutjeharms, J.R.E., 1994. Eddy fluxes of heat and salt from the southwest Indian Ocean into the southeast Atlantic Ocean: a case study. Journal of Geophysical Research 99 (C7), 14053–14070.
Van Geffen, J.H.G.M., Davies, P.A., 2000. A monopolar vortex encounters a north–south ridge or trough. Fluid Dynamics Research 26, 157–179.
Weijer, W., de Ruijter, W.P.M., Sterl, A., Drijfhout, S.S., 2002. Response of the Atlantic overturning circulation to South Atlantic sources of buoyancy. Global and Planetary Change 34, 293–311.
Zavala Sansón, L., Van Heijst, G.J.F., 2000. Interaction of barotropic vortices with coastal topographies: laboratory experiments and numerical simulations. Journal of Physical Oceanography 30 (9), 2141–2162.